Response to reviewer

We thank the reviewer for the constructive comments and suggestions, which are very helpful for the improvement of the manuscript. We have revised the manuscript appropriately and addressed all the reviewer's comments point-by-point for consideration as below. The remarks from the reviewer are shown in black, and our responses are shown in blue color. All the page and line numbers mentioned following are refer to the revised manuscript without change tracked.

The authors have added some new analysis to answer the reviewers' questions, though the overall results seem to be the same as the previous manuscript. There are some additional issues with data processing and HCHO yield calculation, which I think should be addressed carefully before being acceptable for publication:

1. The authors mention the strip patterns are caused by the data processing method they use (Method 2). Using Method 1 could largely remove the strip patterns. It's unclear to me why the authors insist using Method 2 to process data, while Method 1 is clearly much better. I'd suggest the authors use Method 1, otherwise readers will likely interpret the artificial patterns shown in Figure 2 as errors with satellite retrievals.

R: Thanks for the comments. Due to the employment of smoothing procedure in Method 1, the strip patterns were largely removed. We agreed that this kind of strip patterns could be misunderstood as the errors with satellite retrievals. So we finally decided to follow the reviewer's suggestion using Method 1 for the data processing. Except for the strip pattern in spatial distribution, the annual, monthly or seasonal averages for the Shanghai area changed very slight. The relevant figures and reported values were all replaced with the updated one, including Figure 1, 2, 3, 4, 5, 6, 7, 9, 10, Figure S1, and Figure S2. Please refer to the revised manuscript and supplementary.

Moreover, we also want to clarify that the strip patterns were not caused by the Method 2 itself previously, but considered to be inherited from the satellite product without the smoothing procedure.

2. Table R2 is confusing to me. The authors show the HCHO yield from secondary VOCs is higher than primary emission by nearly two orders of magnitude, which doesn't sound right to me. How did you calculate HCHO yield? What is the speciation of VOCs for each sector? More details are needed here.

R: Thanks for the constructive comments. Table R2 in last responses document (RC1) summarized the estimated May-September total HCHO production in eastern China in 2010 from CB05 and SAPRC07 mechanism species, and the comparison with the reference (Shen et al., 2019). We're not sure whether the reviewer want to pointed to Table R1, which listed the primary emissions and estimated secondary productions of HCHO from anthropogenic NMVOCs based on SAPRC07 mechanism species, and showed the secondary production is higher than primary emission by nearly two orders of magnitude.

Here we have replied this concern from three aspects.

(1) Calculation of HCHO yield

Taking year of 2010 as an example, we have detailed described the calculation process of secondary HCHO production as following. The total anthropogenic NMVOCs emission of Shanghai in MEIC is about 58.21×10^4 t, of which industrial, power, residential and transportation is 44.52×10^4, 0.15×10^4, 2.61×10^4 and 10.93×10^4 t, respectively.

Based on the MEIC methodology, the total NMVOCs emission can be split into individual species and then mapped into various chemical mechanisms that are configured in the chemical transport models, such as SAPRC 07, CB05, RACM and GEOS-Chem, etc. (Li et al., 2014). In this study, the total NMVOCs have been speciated into 36 species individually for each sector using SAPRC07 mechanism. Figure R1 shows the speciation of NMVOCs for each sector. For example, there were 5.81×10^9 mol NMVOCs species in total for industry sector, respective to the total emission of 4.452×10^{11} g as mentioned above, the averaged molecular weight for the speciated NMVOCs is about 76.6 g mol^{-1}. So far, no obvious errors in the NMVOCs speciation were found.
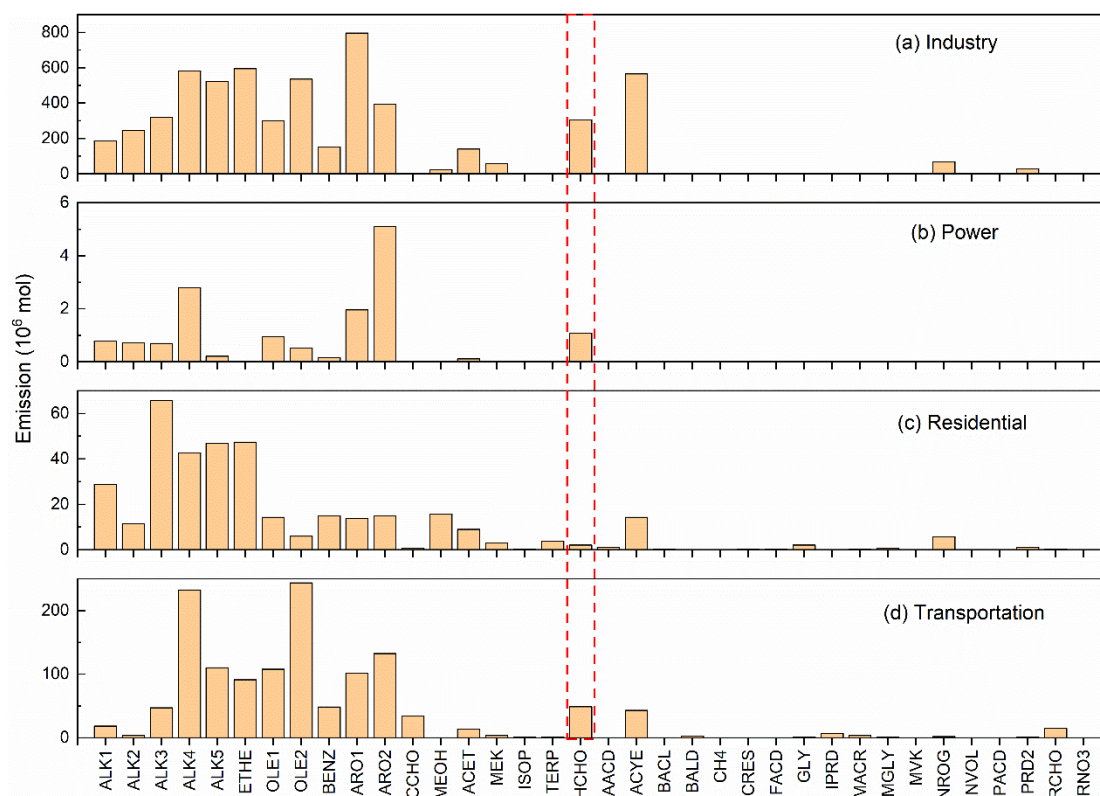

Figure R1. The speciation and emissions of NMVOCs of Shanghai for each sector in 2010.

Then, we can determine the HCHO yield of each species of each sector individually, and summed up to get the secondary HCHO from anthropogenic NMVOCs for a given sector, as expressed in Eq. (R1).

$$S = M_{HCHO} \sum_i E_i n_i Y_i \qquad (R1)$$

where S (unit: g) is the secondary HCHO production from anthropogenic NMVOCs for a given sector, M_{HCHO} (unit: g mol^{-1}) represents the molecular weight of formaldehyde. For each sector, E_i (unit: mol) is the primary emission of NMVOC speciation i, as shown in Figure R1. n_i stands for the number of carbons in the species i. Y_i is the HCHO yield per carbon for species i, as referred to the 1-day HCHO yields under high-NOx conditions from VOCs in Shen et al. (2019).

In order to explain clearly, we used the species emission of acetaldehyde of transportation sector to show the calculation process. In Fig. R1(d), the transportation emitted primarily acetaldehyde (indicated as CCHO in SAPRC07) was 33.91×10^6 mol in 2010. According to the corresponding HCHO yield per carbon (Y_{CCHO}=0.5) and number of carbons in acetaldehyde (n_{CCHO}=2), the secondary HCHO production from acetaldehyde in transportation was calculated to be 1.02×10^9 g. Similarly, all the species for each sector can be further calculated and summed up, as listed in Table S1.

It's important to pointed that the emitted NMVOC species are impossible to be oxidized totally to HCHO, and the calculated secondary production from anthropogenic NMVOC should be overestimated significantly than they actually produced HCHO in the real atmosphere. This results just indicate the potential of anthropogenic secondary production of HCHO, and do not represent the accurate production in the environment. We have also clarified it in the revised manuscript, and please refer to Line 193-194.

2) Quantification of primary emission

As mentioned above, the primary HCHO emission of each sector can be obtained during the speciation procedure, marked with red rectangle in Fig. R1. Meanwhile, we double checked the primary anthropogenic HCHO emission by comparing with some previous literatures, shown in Figure R2. It can prove that the primary anthropogenic HCHO emission only occupied a small proportion in total anthropogenic NMVOC emission in Shanghai (1-2%), Beijing (~3%) and surrounding area (~2%), China (~2%) and the Asia (1-2%). Combined with the total anthropogenic NMVOCs emission of Shanghai, we considered the estimated primary anthropogenic HCHO emission as a reasonable amount.
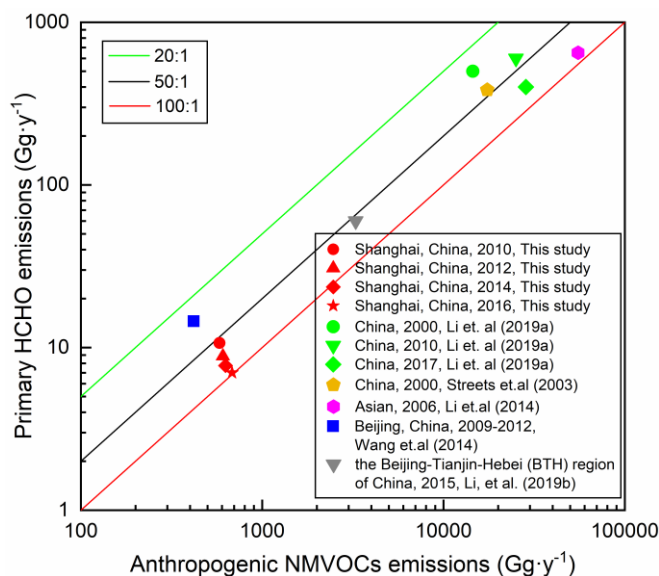
Figure R2. Comparisons of proportion of primary anthropogenic HCHO emissions to total anthropogenic NMVOCs emissions with other studies.

3) Explanations for the huge difference between primary emission and secondary production from anthropogenic NMVOCs.

The above two aspects showed that the primary emission and secondary production of HCHO from anthropogenic NMVOCs were estimated in a reasonable way. But the huge difference between primary emission and secondary production is largely deviated from the common sense as the reviewer suggested.

We think that the amount of primary HCHO emission from anthropogenic is quite reliable compared the overestimated secondary production. In the calculation of secondary production from anthropogenic NMVOC, we used the HCHO yield from Shen et al. (2019), which is computed for 1-day HCHO yields under high-NO_x conditions from VOCs and comparable with other studies (Chan Miller et al., 2016; Zhu et al., 2014). However, not all the primary anthropogenic NMVOCs are engaged in the reaction to form HCHO, this calculated secondary production just stands for the potential, not the real production or contribution.

In addition, we have to stated that previous studies of HCHO attempting to unravel the role of secondary production versus direct emission vary widely in their estimates and the conclusions are varied in spatial and temporal (e.g. Luecken et al., 2018; Stroud et al., 2016; Ling et al., 2017; Liu et al., 2020). In addition, even for the same area but different techniques, the secondary production of total HCHO were determined from 30-50% to 95% (and mostly point sources 92%) (Zhang et al., 2013; Parrish et al., 2012). Therefore, the exact conclusion about the ratio of HCHO yielded from secondary production of VOCs to primary emission is difficult to drawn from the existing discussions in this study, and the possibility of such magnitude differences can not be excluded completely neither.

3. The authors show secondary production of HCHO is over 30 times higher for anthropogenic emissions (300 * 10^9 g) than biogenic emissions (9 * 10^9 g). This shouldn't be right. We know that globally biogenic emissions are the largest contributor to HCHO. Even for urban areas, the contribution from anthropogenic vs. biogenic emissions should be comparable. I'd suggest the authors double check their methods for calculating HCHO yield, which may also explain my previous question.

R: Thanks for the constructive comments. In view of the HCHO columns, they are commonly found in large quantities over forested regions in the world, however, a large fraction of HCHO columns was observed in industrial/urban regions in East Asia, that HCHO levels were 19-33% higher in urban regions than forested regions (Souri et al., 2017). While the biogenic emissions are contributed significantly to HCHO in global scale, large values of HCHO observed in megacities indicate the predominance of anthropogenic sources.

Figure R3 displays the land surface type of Shanghai, which shows the high degree of urbanization and less coverage of broadleaf trees. Broadleaf trees are considered the biggest contributor to isoprene, while crops are weak isoprene emitters (Stavrakou et al., 2014; Li et al., 2016). We have also added Figure R3 as Figure S3 in the supplementary. Therefore, in such an urbanized and densely populated megacity Shanghai, the biogenic VOC emissions are expected to be much minor compared to forested regions (Liu et al., 2018; Wu et al., 2020a; Li et al., 2020). The biogenic VOCs emissions about 1.2×10^4 t of Shanghai in 2014, used to infer the HCHO yields, is comparable with the reported values in those literatures. Therefore, we would not expect more HCHO yield from biogenic emission than current estimation.
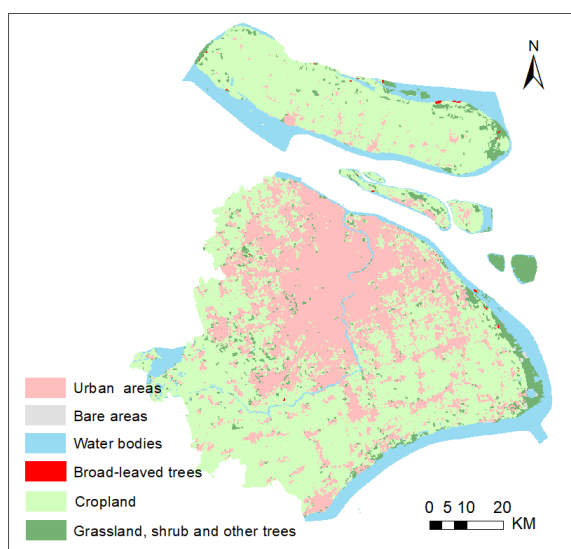

Figure R3. The spatial distribution of surface land types in Shanghai (data from ESA Land Cover Product, available at: http://maps.elie.ucl.ac.be/CCI/viewer/).

So we think the contribution to HCHO of biogenic emissions may not be comparable to anthropogenic sources in Shanghai. In Beijing-Tianjin-Heibei area of China, the

anthropogenic VOCs might impose substantial impacts more, especially in urbanized areas (Zhu et al., 2018). Based on the two models (the Positive Matrix Factorization (PMF) model and a photochemical box model with Master Chemical Mechanism (PBM-MCM)), the contribution of isoprene, indicating the biogenic emission, to secondary HCHO formation was about 9.6± 3% in July 2006 at an urban site in the Pearl River Delta (PRD), China, much lower than that at semi-rural site in Guangzhou about 43.2% (Ling et al., 2017). It suggested the contribution of biogenic emissions to secondary HCHO production in urban site may not be important as much as expected like other places, even in summer season.

Finally, we would like to conclude that the secondary production plays a dominant role for HCHO compared to direct emission, however, the relative importance of anthropogenic or biogenic emission contributed to secondary production are still in disputed, which is strongly associated to the time and location, and the results also will be impacted by the adopted methodology (e.g. Wang et al., 2017; Bastien et al., 2019; Wu et al., 2020b). The quantifications of specific anthropogenic source types or VOC precursors contributing to HCHO have less been done so far, need to be further investigated.

Back to the manuscript context, we used the primary emission of HCHO from MEIC in the initial submission, in order to justify the impacts of anthropogenic directly emissions. As the reviewer suggested, we should not overlook the important secondary production. So we have estimated roughly the secondary production from anthropogenic and biogenic emissions. This is a very insightful comments and we do want to take more efforts on this issue which are not well explained by others. But considering the main focus of the manuscript, we would appreciate reviewer's understanding that we would not discuss too much regarding whether the secondary production from biogenic or anthropogenic contribute more. We hope this manuscript can prompt the perspective on the inferring ozone sensitivity from satellite HCHO/NO$_2$ ratio revised with ground surface measurement.

References:

Bastien, L. A. J., Brown, N. J., and Harley, R. A.: Contributions to local- and regional-scale formaldehyde concentrations, Atmos Chem Phys, 19, 8363-8381, https://doi.org/10.5194/acp-19-8363-2019, 2019.

Chan Miller, C., Jacob, D. J., González Abad, G., and Chance, K.: Hotspot of glyoxal over the Pearl River delta seen from the OMI satellite instrument: implications for emissions of aromatic hydrocarbons, Atmos. Chem. Phys., 16, 4631–4639, https://doi.org/10.5194/acp-16-4631-2016, 2016.

Li, M., Zhang, Q., Streets, D. G., He, K. B., Cheng, Y. F., Emmons, L. K., Huo, H., Kang, S. C., Lu, Z., Shao, M., Su, H., Yu, X., and Zhang, Y.: Mapping Asian anthropogenic emissions of non-methane volatile organic compounds to multiple chemical mechanisms, Atmos Chem Phys, 14,

5617-5638, https://doi.org/10.5194/acp-14-5617-2014, 2014.

Li, J., Li, L. Y., Wu, R. R., Li, Y. Q., Bo, Y., and Xie, S. D.: Inventory of highly resolved temporal and spatial volatile organic compounds emission in China, in: Air Pollution Xxiv, edited by: Longhurst, J. W. S., Brebbia, C. A., and Barnes, J., WIT Transactions on Ecology and the Environment, 79-86, 2016.

Li, M., Zhang, Q., Zheng, B., Tong, D., Lei, Y., Liu, F., Hong, C. P., Kang, S. C., Yan, L., Zhang, Y. X., Bo, Y., Su, H., Cheng, Y. F., and He, K. B.: Persistent growth of anthropogenic non-methane volatile organic compound (NMVOC) emissions in China during 1990-2017: drivers, speciation and ozone formation potential, Atmos Chem Phys, 19, 8897-8913, https://doi.org/10.5194/acp-19-8897-2019, 2019a.

Li, J., Hao, Y. F., Simayi, M., Shi, Y. Q., Xi, Z. Y., and Xie, S. D.: Verification of anthropogenic VOC emission inventory through ambient measurements and satellite retrievals, Atmos Chem Phys, 19, 5905-5921, https://doi.org/10.5194/acp-19-5905-2019, 2019b.

Li, L. Y., Yang, W. Z., Xie, S. D., and Wu, Y.: Estimations and uncertainty of biogenic volatile organic compound emission inventory in China for 2008-2018, Sci Total Environ, 733, https://doi.org/10.1016/j.scitotenv.2020.139301, 2020.

Ling, Z. H., Zhao, J., Fan, S. J., and Wang, X. M.: Sources of formaldehyde and their contributions to photochemical O_3 formation at an urban site in the Pearl River Delta, southern China, Chemosphere, 168, 1293-1301, https://doi.org/10.1016/j.chemosphere.2016.11.140, 2017.

Liu, Y., Li, L., An, J. Y., Huang, L., Yan, R. S., Huang, C., Wang, H. L., Wang, Q., Wang, M., and Zhang, W.: Estimation of biogenic VOC emissions and its impact on ozone formation over the Yangtze River Delta region, China, Atmos Environ, 186, 113-128, https://doi.org/10.1016/j.atmosenv.2018.05.027, 2018.

Liu, Y., Tang, Z. P., Abera, T., Zhang, X. Z., Hakola, H., Pellikka, P., and Maeda, E.: Spatio-temporal distribution and source partitioning of formaldehyde over Ethiopia and Kenya, Atmos Environ, 237, 9, https://doi.org/10.1016/j.atmosenv.2020.117706, 2020.

Luecken, D. J., Napelenok, S. L., Strum, M., Scheffe, R., and Phillips, S.: Sensitivity of Ambient Atmospheric Formaldehyde and Ozone to Precursor Species and Source Types Across the United States, Environ Sci Technol, 52, 4668-4675, https://doi.org/10.1021/acs.est.7b05509, 2018.

Parrish, D. D., Ryerson, T. B., Mellqvist, J., Johansson, J., Fried, A., Richter, D., Walega, J. G., Washenfelder, R. A., de Gouw, J. A., Peischl, J., Aikin, K. C., McKeen, S. A., Frost, G. J., Fehsenfeld, F. C., and Herndon, S. C.: Primary and secondary sources of formaldehyde in urban atmospheres: Houston Texas region, Atmos Chem Phys, 12, 3273-3288, https://doi.org/10.5194/acp-12-3273-2012, 2012.

Shen, L., Jacob, D. J., Zhu, L., Zhang, Q., Zheng, B., Sulprizio, M. P., Li, K., De Smedt, I., Abad, G. G., Cao, H. S., Fu, T. M., and Liao, H.: The 2005-2016 Trends of Formaldehyde Columns Over China Observed by Satellites: Increasing Anthropogenic Emissions of Volatile Organic Compounds and Decreasing Agricultural Fire Emissions, Geophys Res Lett, 46, 4468-4475, https://doi.org/10.1029/2019gl082172, 2019.

Souri, A. H., Choi, Y., Jeon, W., Woo, J. H., Zhang, Q., and Kurokawa, J.: Remote sensing evidence of decadal changes in major tropospheric ozone precursors over East Asia, J. Geophys. Res.-Atmos., 122, 2474-2492, https://doi.org/10.1002/2016jd025663, 2017.

Stavrakou, T., Muller, J. F., Bauwens, M., De Smedt, I., Van Roozendael, M., Guenther, A., Wild, M., and Xia, X.: Isoprene emissions over Asia 1979-2012: impact of climate and land-use changes, Atmos. Chem. Phys., 14, 4587-4605, https://doi.org/10.5194/acp-14-4587-2014, 2014.

Streets, D. G., Bond, T. C., Carmichael, G. R., Fernandes, S. D., Fu, Q., He, D., Klimont, Z., Nelson, S. M., Tsai, N. Y., Wang, M. Q., Woo, J. H., and Yarber, K. F.: An inventory of gaseous and primary aerosol emissions in Asia in the year 2000, J. Geophys. Res.-Atmos., 108, https://doi.org/10.1029/2002jd003093, 2003.

Stroud, C. A., Zaganescu, C., Chen, J., McLinden, C. A., Zhang, J. H., and Wang, D.: Toxic volatile organic air pollutants across Canada: multi-year concentration trends, regional air quality modelling and source apportionment, Journal of Atmospheric Chemistry, 73, 137-164, https://doi.org/10.1007/s10874-015-9319-z, 2016.

Wang, M., Shao, M., Chen, W., Yuan, B., Lu, S., Zhang, Q., Zeng, L., and Wang, Q.: A temporally and spatially resolved validation of emission inventories by measurements of ambient volatile organic compounds in Beijing, China, Atmos Chem Phys, 14, 5871-5891, https://doi.org/10.5194/acp-14-5871-2014, 2014.

Wang, C., Huang, X. F., Han, Y., Zhu, B., and He, L. Y.: Sources and Potential Photochemical Roles of Formaldehyde in an Urban Atmosphere in South China, J. Geophys. Res.-Atmos., 122, 11934-11947, https://doi.org/10.1002/2017jd027266, 2017.

Wu, K., Yang, X. Y., Chen, D., Gu, S., Lu, Y. Q., Jiang, Q., Wang, K., Ou, Y. H., Qian, Y., Shao, P., and Lu, S. H.: Estimation of biogenic VOC emissions and their corresponding impact on ozone and secondary organic aerosol formation in China, Atmos Res, 231, https://doi.org/10.1016/j.atmosres.2019.104656, 2020a.

Wu, C., Wang, C., Wang, S., Wang, W., Yuan, B., Qi, J., Wang, B., Wang, H., Wang, C., Song, W., Wang, X., Hu, W., Lou, S., Ye, C., Peng, Y., Wang, Z., Huangfu, Y., Xie, Y., Zhu, M., Zheng, J., Wang, X., Jiang, B., Zhang, Z., and Shao, M.: Measurement report: Important contributions of oxygenated compounds to emissions and chemistry of volatile organic compounds in urban air, Atmos. Chem. Phys., 20, 14769–14785, https://doi.org/10.5194/acp-20-14769-2020, 2020b.

Zhang, H. L., Li, J. Y., Ying, Q., Guven, B. B., and Olaguer, E. P.: Source apportionment of formaldehyde during TexAQS 2006 using a source-oriented chemical transport model, J. Geophys. Res.-Atmos., 118, 1525-1535, https://doi.org/10.1002/jgrd.50197, 2013.

Zhu, L., Jacob, D. J., Mickley, L. J., Marais, E. A., Cohan, D. S., Yoshida, Y., Duncan, B. N., Abad, G. G., and Chance, K. V.: Anthropogenic emissions of highly reactive volatile organic compounds in eastern Texas inferred from oversampling of satellite (OMI) measurements of HCHO columns, Environ Res Lett, 9, 7, https://doi.org/10.1088/1748-9326/9/11/114004, 2014.

Zhu, S. Y., Li, X. Y., Yu, C., Wang, H. M., Wang, Y. P., and Miao, J.: Spatiotemporal Variations in Satellite-Based Formaldehyde (HCHO) in the Beijing-Tianjin-Hebei Region in China from 2005 to 2015, Atmosphere-Basel, 9, 24, https://doi.org/10.3390/atmos9010005, 2018.

OMI-observed HCHO in Shanghai, China during 2010-2019 and ozone sensitivity inferred by improved HCHO/NO₂ ratio

Danran Li [1], Shanshan Wang [1,2], Ruibin Xue [1], Jian Zhu [1], Sanbao Zhang[1], Zhibin Sun[1], and Bin Zhou [1,2,3]

5 [1]Shanghai Key Laboratory of Atmospheric Particle Pollution and Prevention (LAP[3]), Department of Environmental Science and Engineering, Fudan University, Shanghai, China
[2]Institute of Eco-Chongming (IEC), No. 20 Cuiniao Road, Shanghai 202162, China
[3]Institute of Atmospheric Sciences, Fudan University, Shanghai, 200433, China

Correspondence to: Shanshan Wang (shanshanwang@fudan.edu.cn)

10 **Abstract.** In recent years, satellite remote sensing has been increasingly used in the long-term observation of ozone (O₃) precursors and its formation regime. In this work, formaldehyde (HCHO) data from Ozone Monitoring Instrument (OMI) were used to analyse the temporal and spatial distribution of HCHO vertical column densities (VCDs) in Shanghai from 2010 to 2019. HCHO VCDs exhibited the highest value in summer and the lowest in winter, the high-VCD concentrated in western Shanghai. Temperature largely influence HCHO by affecting the biogenic emissions and photochemical reactions, 15 and industry was the major anthropogenic source. The satellite observed formaldehyde to nitrogen dioxide ratio (FNR$_{SAT}$) reflects that the O₃ formation regime had significant seasonal characteristics and gradually manifested as transitional ozone formation regime dominated in Shanghai. The uneven distribution in space was mainly reflected as the higher FNR$_{SAT}$ and surface O₃ concentration in suburban area. To compensate the shortcoming of FNR$_{SAT}$ that it can only characterize O₃ formation around satellite overpass time, correction of FNR$_{SAT}$ was implemented with hourly surface FNR and O₃ data. 20 After correction, O₃ formation regime showed the trend moving towards VOC-limited in both time and space, and regime indicated by FNR$_{SAT}$ can better reflect O₃ formation for a day. This study can help us better understand HCHO characteristics and O₃ formation regime in Shanghai, and also provide a method to improve FNR$_{SAT}$ for characterizing O₃ formation in a day, which will be significant for developing O₃ prevention and control strategies.

1 Introduction

25 Formaldehyde (HCHO) is an important trace gas in atmosphere. It has the irritating effect on human eyes, skin, and respiratory mucosa, and can also cause cancer in high concentration (Zhu et al., 2017a; Liu et al., 2018a). Atmospheric HCHO is an intermediate product of almost all volatile organic compounds (VOCs) oxidation, it can be therefore indicative of the overall VOCs level (Chan et al., 2019). HCHO can also be emitted through anthropogenic sources, biogenic sources, and biomass combustion. Anthropogenic sources like transportation, power, industry, and residential etc. increase the 30 amount of HCHO by emitting VOCs into the atmosphere (Wang et al., 2017). In addition, biogenic volatile organic

1

compounds (BVOCs) are also important sources of HCHO. Isoprene emitted by plant can be oxidized to generate HCHO, which causes the concentration of HCHO in some lush vegetation areas to be largely affected by emission of BVOCs (Millet et al., 2008). The removal of HCHO is mainly through photolysis, reaction with OH radicals and the deposition (Ling et al., 2016; Xing et al., 2020).

35   Satellite remote sensing can achieve large-scale observation of atmospheric pollutant gases including HCHO, which has been widely used in recent years. Sensors currently available for HCHO observation include the Global Ozone Monitoring Experiment (GOME) on ERS-2 (Burrows et al., 1999; Martin et al., 2004b), Scanning Imaging Absorption Spectrometer for Atmospheric Chartography (SCIAMACHY) on ENVISAT (Bovensmann et al., 1999; Stavrakou et al., 2009), Ozone Monitoring Instrument (OMI) on Aura (Levelt et al., 2006; Zhu et al., 2017b), GOME-2 A, B, and C on METOP as the

40   successor of GOME (Callies et al., 2000; De Smedt et al., 2012), Ozone Mapping and Profiler Suite (OMPS) on Suomi-NPP (Su et al., 2019), and Tropospheric Monitoring Instrument (TROPOMI) on Sentinel-5P (Veefkind et al., 2012; Vigouroux et al., 2020). OMI can provide daily data of HCHO with higher spatial resolution (13 km×24 km). As a new generation of sensors, TROPOMI was launched in 2017, it has better spatial resolution (7 km×7 km) but lacks long-term observation so far. It would be an advantageous tool of satellite remote sensing to achieve more detailed analysis in the future (Veefkind et al.,

45   2012).

Previous studies reported satellite observed long-term and large-scale distribution and variation of HCHO in China and all over the world (Millet et al., 2008; Zhu et al., 2017a; Liu et al., 2020). Twelve years observation of multi-satellite (OMI, GOME-2, SCIAMACHY) showed that the trend of HCHO vertical column densities (VCDs) over eastern China is consistent with that of anthropogenic VOCs (Shen et al., 2019). Based on 10 years observation of OMI HCHO, Liu et al.

50   (2018a) indicated that high HCHO VCDs in tropical forests region are greatly affected by biomass burning and meteorological factors including temperature and precipitation. In addition, the ground-based remote sensing can also be available for HCHO observation, such as the multi axis differential optical absorption spectroscopy (MAX-DOAS) measurement. The vertical distribution of HCHO derived from MAX-DOAS measurement was characterized by the higher HCHO concentrated near the surface (Lee et al., 2015; Chan et al., 2019). By employing the box model, Li et al. (2014)

55   found that isoprene oxidation initiated by OH radicals have a great contribution to the HCHO formation in semi-rural region of the Pearl River Delta (PRD) in China.

HCHO participates in the complex photochemical reaction of NO_x (NO_x= NO + NO_2) and directly affects the production of O_3 in troposphere. Due to the short lifetime of HCHO and NO_2, their spatial distributions were greatly affected by local emission of VOCs and NO_x, which received widespread attention as precursors of tropospheric O_3 (Zaveri et al., 2003; Chan

60   et al., 2019). Consequently, HCHO and NO_2 can be assumed as indicators of VOCs and NO_x, and the ratio of formaldehyde to nitrogen dioxide (HCHO/NO_2, FNR) can be an indicator to analyse the O_3 formation regime (Sillman, 1995; Martin et al., 2004a; Schroeder et al., 2017). For instance, by using FNR from long-term OMI HCHO and NO_2 data, O_3 sensitivity of the United States was evaluated. O_3 formation regime can be designated as VOC-limited for FNR < 1, NO_x-limited for FNR > 2, and transition for 1 < FNR < 2, which serves as the transitional regime between VOC-limited and NO_x-limited regimes,

2

65 indicating the production of O$_3$ can be changed by both VOC and NO$_x$ (Duncan et al., 2010). In view of China, OMI products over three representative regions (North China Plain (NCP), the Yangtze River Delta (YRD) and the PRD) were investigated, revealing that the O$_3$ formation regime varied in both time and space, and the contribution of emission sectors to precursors changed with the type of regimes (Jin and Holloway, 2015). During special events such as Asia-Pacific Economic Cooperation in 2014 and Grand Military Parade in 2015, FNR in Beijing had become higher compared with

70 previous periods, and the O$_3$ formation regime shifted toward NO$_x$-limited regime with control strategies (Liu et al., 2016). In this study, OMI satellite data were used to investigate the temporal and spatial distribution characteristics of atmospheric HCHO in Shanghai from 2010 to 2019, combined with meteorological data and emission inventories to analyse the influencing factors. FNR calculated by satellite HCHO and NO$_2$ were applied to capture variation of the O$_3$ formation regime in Shanghai over the past decade. Considering that satellite data only reflect the column density of trace gas around overpass

75 time, hourly surface FNR and O$_3$ concentration increment were proposed to correct the satellite FNR, so that it can better indicate O$_3$ formation in the daytime.

2 Data and Methods

2.1. Satellite data

OMI on Aura orbits the earth in about 98 minutes, which can achieve full coverage of the earth in one day. It overpasses at

80 13:45 local time (LT) each day. The scanning width is 2600 km, and is divided into 60 rows. The sensor contains 3 channels, including UV-1, UV-2, and VIS, with a wavelength coverage of 264-504 nm. This band allows to observe a variety of trace gases, e.g., HCHO, NO$_2$, and SO$_2$ (Zhang et al., 2019). The retrieval algorithm of this product is based on nonlinear least-squares fitting which get slant column density (SCD) as the result. Then SCD can be converted to VCD through Air Mass Factors (AMF). The Level-2 OMI HCHO product OMHCHO Version-3 is used in this study (https://disc.gsfc.nasa.gov).

85 Since atmospheric HCHO is mainly distributed in the troposphere, the total VCD can be regarded as the tropospheric VCD of HCHO (Duncan et al., 2010). The Level-2 OMI NO$_2$ product OMNO2.003 Version-4 is adopted as tropospheric NO$_2$ VCD in this study (https://disc.gsfc.nasa.gov).

2.2. Methodology

In this study, Shanghai and surrounding areas were gridded into to a spatial resolution of 0.01°×0.01°., Then pixel falling

90 within a 24 km radius of the grid center were averaged, and further was assigned to that grid (Fioletov et al., 2011; McLinden et al., 2012; Zhu et al., 2014).HCHO VCD of each pixel was assigned to the respective grid by determining the coordinates information. Weight function including cloud function and pixel size was introduced to effectively improve the quality of processed data (Xue et al., 2020). In order to remove data with poor quality as much as possible, HCHO data with cloud fraction ≤ 30%, solar zenith angle ≤ 70°, and Main Data Quality Flag = 0 were selected in this study. In addition, the

95 quality of pixel data with large size is poor, so 5 marginal pixels on each side were abandoned, and only pixel data within

3

6~55 were selected (Zhu et al., 2017a; Xue et al., 2020). Because OMI has experienced row anomaly since 2007, Xtrack flag = 0 was required to eliminate the influence of poor quality data affected by row anomaly (http://projects.knmi.nl/omi/research/product/rowanomaly-background). As HCHO satellite data have large error, fitting root mean square (RMS) $\leq$ 0.003 was limited to remove most outliers (Souri et al., 2017). The selection of NO_2 satellite data was basically the same as that of HCHO, but without fitting RMS parameter filtering, and cloud radiance fraction $\leq$30% was required (Krotkov et al., 2016; Xue et al., 2020). Moreover, the linear regressions of monthly deseasonalized zonal mean HCHO VCDs with 0.5° latitude steps over remote pacific region (29° - 33 °N, 160° - 140 °W) indicated that OMI HCHO product used in this study do not show the obvious drift (Zhu et al., 2017b).

2.3. Auxiliary data

The meteorological data, including monthly temperature, sunshine hours, precipitation, and relative humidity are acquired from the National Bureau of Statistics of China (http://www.stats.gov.cn/). Hourly temperature data at Shanghai Hongqiao INTL Site (31.20°N, 121.34°E) come from the National Climatic Data Center (NCDC, https://www.ncdc.noaa.gov/). The anthropogenic sources of HCHO in Shanghai are calculated based on the Multi-resolution Emission Inventory for China (MEIC, http://www.meicmodel.org/). Surface HCHO and NO_2 concentrations were measured by long-path differential optical absorption spectroscopy (LP-DOAS) at the Jiangwan campus of Fudan University in Shanghai (31.34°N, 121.52°E). The O_3 data of Qingpu Dianshan Lake Site (31.09°N, 120.98°E) and Hongkou Site (31.30°N, 121.47°E) in Shanghai are obtained from the Shanghai Environmental Monitoring Center (http://www.semc.com.cn/aqi/Home/Index).

3. Results and Discussion

3.1. The temporal and spatial variation of HCHO

HCHO VCDs for annual, monthly and seasonal variations in Shanghai from 2010 to 2019 are shown in Fig. 1. HCHO VCDs decreased from the highest value of 12.78×10^{15} molec·cm^{-2} in 2010 to the lowest value of 10.39×10^{15} molec·cm^{-2} in 2012, then rebounded from 2012 to 2014, and fluctuated slightly in the following years (Fig. 1a). The column value and variation are similar to previous study in the YRD, China (Zhang et al., 2019). Before 2018, the high-VCD concentrated in June to August for about 15×10^{15} to 20×10^{15} molec·cm^{-2}, the low-VCD appeared in January to February and November to December for about 3×10^{15} to 9×10^{15} molec·cm^{-2}, and VCDs were comparable in remaining months (Fig. 1b). In addition, the amplitude of monthly HCHO VCDs was relatively smaller in 2018 and 2019, and mainly concentrated from 6×10^{15} to 15×10^{15} molec·cm^{-2}. The HCHO VCDs varied with the season, the maxima and minima corresponding to the respective summer (June, July and August) and winter (December, January and February), whereas moderate levels in spring (March, April and May) and autumn (September, October and November) (Fig. 1c). Previous MAX-DOAS and OMI observations also exhibited the same seasonal patterns of HCHO in the YRD, China (Jin and Holloway, 2015; Chan et al., 2019). High temperature and abundant radiation are conducive to the plant growth to produce BVOCs and the photochemical reaction of

4

VOCs, which boost the HCHO formation in summer (Sharkey and Loreto, 1993; Duncan et al., 2009; Narumi et al., 2009). Thus, HCHO VCDs would be relatively low in winter under the opposite weather conditions.
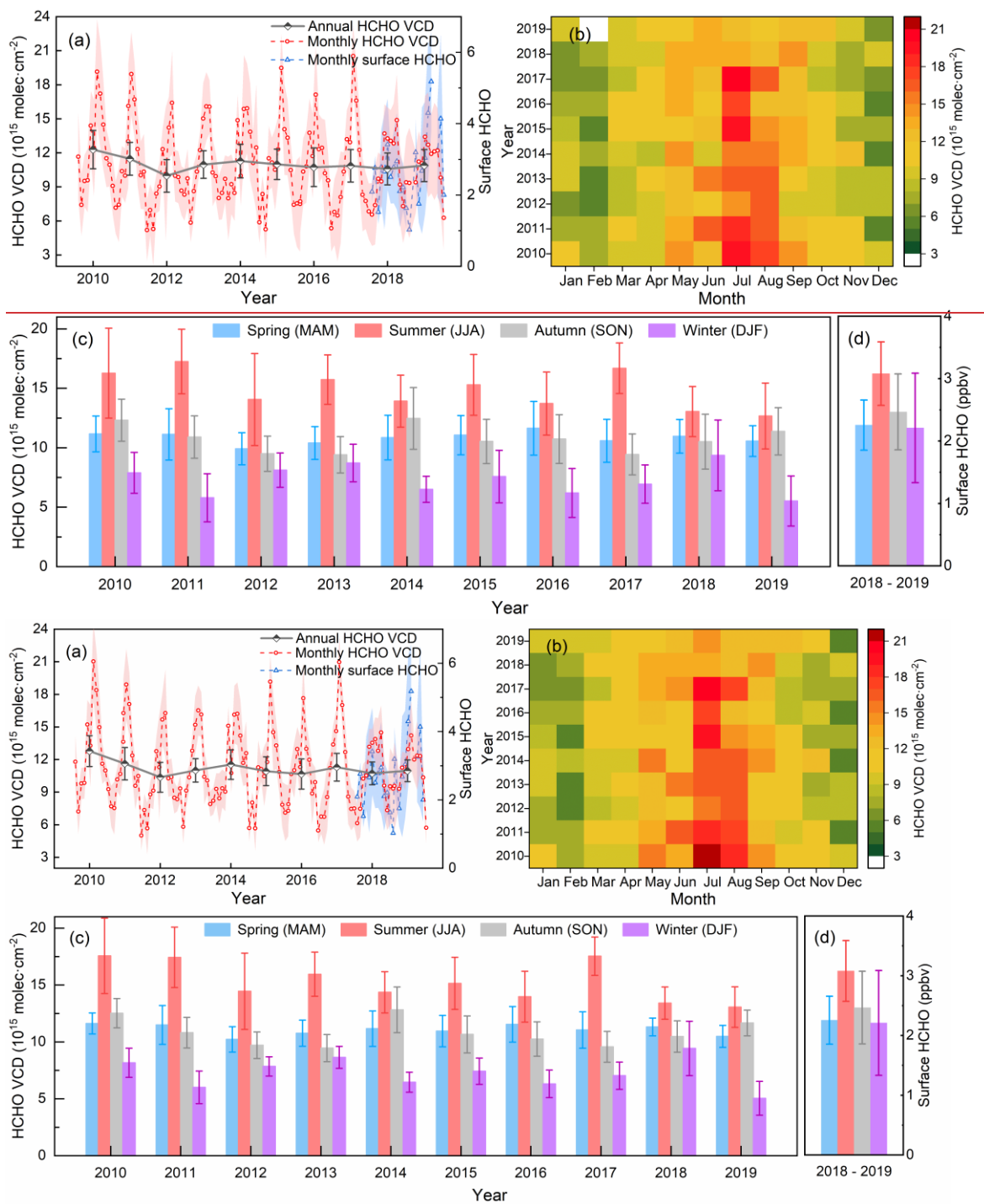

130

Figure 1. OMI and LP-DOAS observed time series of HCHO in Shanghai. (a) to (c) reflect the annual, monthly and seasonal variations of HCHO VCD during 2010-2019, (d) reflects the seasonal variation of surface HCHO during 2018-2019.

The HCHO VCDs within 10 km of LP-DOAS measurement site were averaged to compare with the surface HCHO between 13:00 and 14:00 (Fig. S1). It shows that HCHO VCDs and surface HCHO concentrations are not consistent very well, as

135 HCHO is not completely concentrated near the ground, but has a high concentration at higher altitudes (Chan et al., 2019; Wang et al., 2019). Spatial heterogeneity of surface HCHO in horizontal can also impact the consistency of the comparison. However, the surface HCHO observed by LP-DOAS shows the same seasonal characteristics as HCHO VCDs (Fig. 1d).

The spatial distribution of 10-year averaged HCHO VCD was given in Fig. 2a. In general, HCHO VCDs in eastern coastal area were relatively low, with the level of about 10×10^{15} molec·cm^{-2}. While those in western regions adjacent to other

140 provinces were relatively higher, about 13×10^{15} molec·cm^{-2}. Noted that area with the highest HCHO VCD in Shanghai not appeared in the city center (marked by the red box) but in the relatively remote Qingpu (QP) district, followed by Songjiang (SJ) and Jinshan (JS) district. Compared to the anthropogenic Non-methane volatile organic compounds (NMVOCs) emissions, the distribution of HCHO VCDs does not show the same spatial pattern (An et al., 2021). The high HCHO in western Shanghai were frequently observed and may be explained by the transport of air masses containing high

145 concentrations of reactive VOCs sometimes from Zhejiang and Jiangsu provinces and the significant contribution of local biogenic isoprene to HCHO (Su et al., 2019; Zhang et al., 2020; Zhang et al., 2021).

Figure 2b shows the difference of HCHO VCDs between 2019 and 2010. It suggests that except for the eastern and southern coastal areas, as well as the eastern area of Chongming Island, HCHO VCDs in Shanghai showed an overall downward trend during the past 10 years, with western regions~~Qingpu district~~ experiencing the largest decline. Figure 2c to Fig. 2f display

150 the spatial distribution of HCHO VCDs in different seasons. HCHO VCD in summer was basically above 12×10^{15} molec·cm^{-2}. In winter, the value was around 7×10^{15} molec·cm^{-2} for most regions except for Qingpu district. While in spring and autumn, it was in the moderate level of about 10×10^{15} molec·cm^{-2}. The spatial distribution of HCHO VCDs in different seasons was similar to the 10-year averaged characteristics of high-value in the west and low-value in the east.
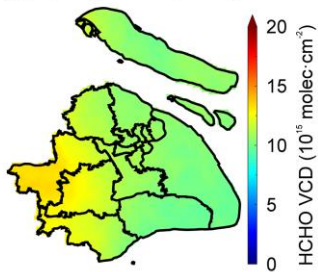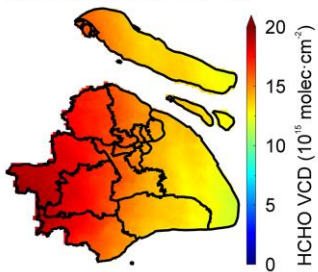
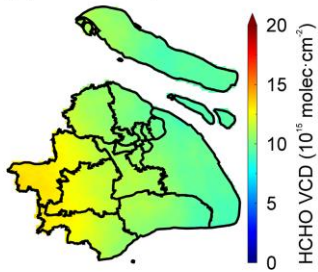(a) Average 2010-2019
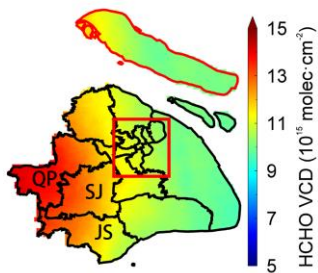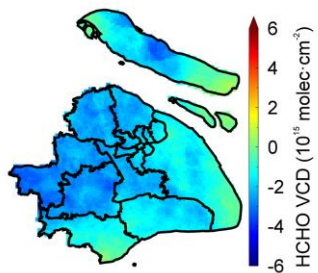
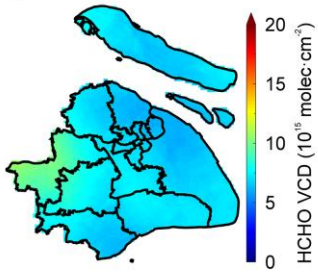(b) Difference 2019-2010

(c) Spring Mar-Apr-May

(d) Summer Jun-Jul-Aug

(e) Autumn Sep-Oct-Nov

(f) Winter Dec-Jan-Feb

(a) Average 2010-2019
(b) Difference 2019-2010
(c) Spring Mar-Apr-May
(d) Summer Jun-Jul-Aug
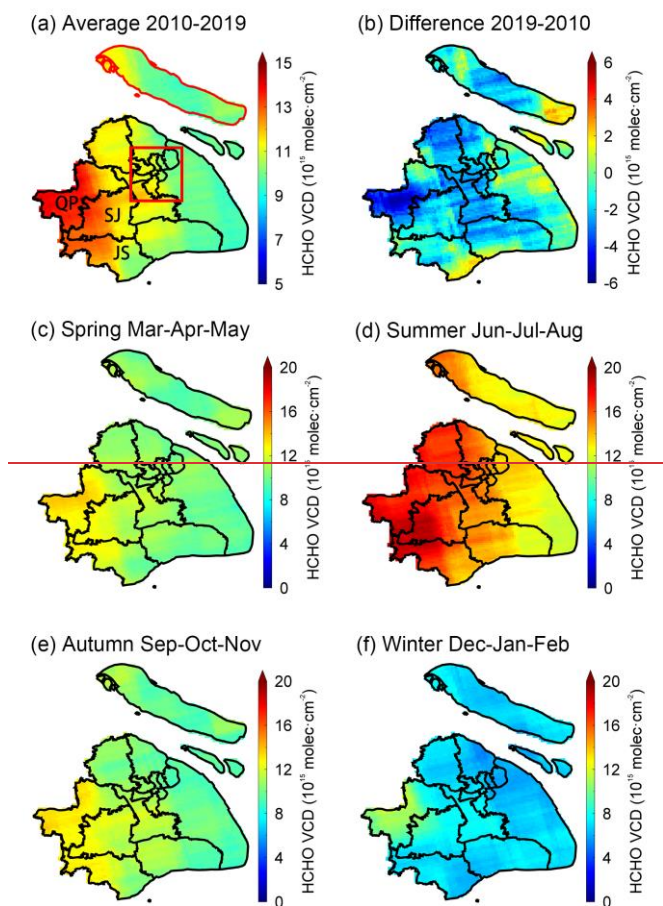**(e) Autumn Sep-Oct-Nov**
(f) Winter Dec-Jan-Feb

155

Figure 2. Spatial distribution of HCHO VCDs in Shanghai: (a) average HCHO VCD for 10 years, (b) the difference of HCHO VCDs between 2019 and 2010 (2019 minus 2010), and (c) to (f) for different seasons. In Fig. 2a the city center is marked with red box, Chongming Island is displayed with red boundary, QP, SJ, and JS refer to Qingpu, Songjiang, and Jinshan district.

3.2. Influencing factors

160   The relationship between monthly HCHO VCDs and meteorological variables including temperature, sunshine hours, precipitation, and relative humidity were analysed via the linear regression. The stepwise regression results show that only temperature correlated with HCHO VCDs significantly among these four meteorological factors. The linear regression of temperature contribution and HCHO VCD was shown in Fig. 3. The temperature contribution has a good correlation with the observed HCHO VCD ($R^2 = 0.7\underline{3}\sout{2}$), which means that temperature can explain about 7$\underline{3}\sout{2}$% of the variation of HCHO VCD.

165   The remaining part that cannot be explained by temperature appears in the form of residual, which is considered as the influence of other changing factors such as anthropogenic emissions (Li et al., 2019). The residual in summer in some years would be particularly large, which indicates that in addition to temperature, there are other factors affecting HCHO VCD significantly.
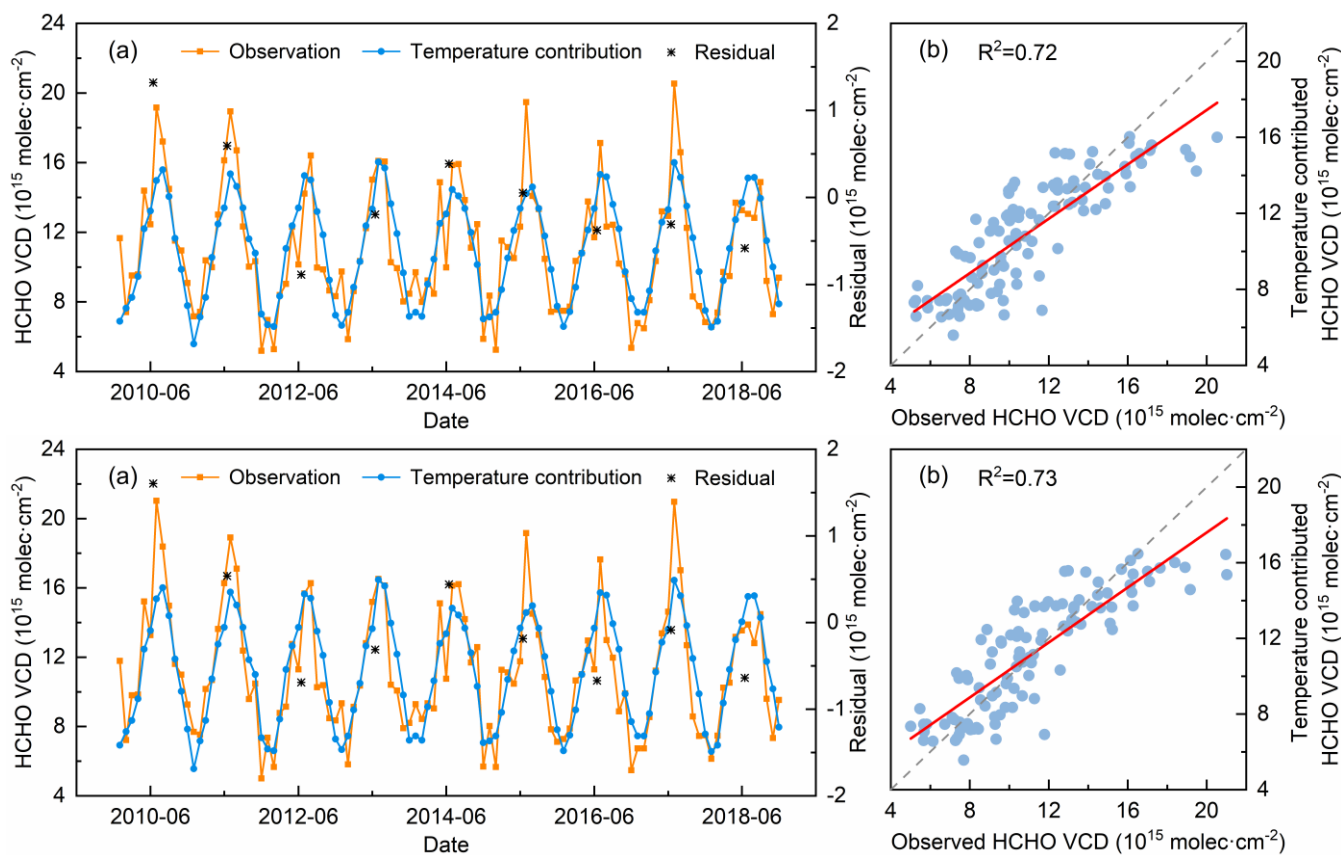
8

Figure 3. Monthly HCHO VCDs and the temperature contribution in Shanghai during 2010-2018. (a) reflects the temporal variations and (b) illustrates the correlation analysis. The black points represent the annual average residuals.

175　The precipitation and relative humidity reached peak in June, while the sunshine hours reached the dip, and HCHO VCD declined with the temperature rose (Fig. S2). Shanghai has a subtropical monsoon climate with rain and heat in the same period. Abundant precipitation largely favoured the wet deposition of HCHO and offset the impact of rising temperature, resulting in a small decrease in HCHO VCDs in June (Pang et al., 2009). The result of Fisher's exact test also illustrates that when the relative humidity changes remarkably, the variation of HCHO VCDs in summer would be significantly affected (P

180　<0.05).

　　To explore the impacts of anthropogenic sources on HCHO abundance, primary emissions and secondary productions of HCHO from anthropogenic sources were estimated. NMVOCs emissions from MEIC v.1.3 grid inventories for the year of 2010, 2012, 2014, and 2016 were mapped to SAPRC07 mechanism species. Primary HCHO was directly obtained from the inventory, secondary HCHO production was calculated based on 1-day HCHO yields of several NMVOCs under high-NO_x
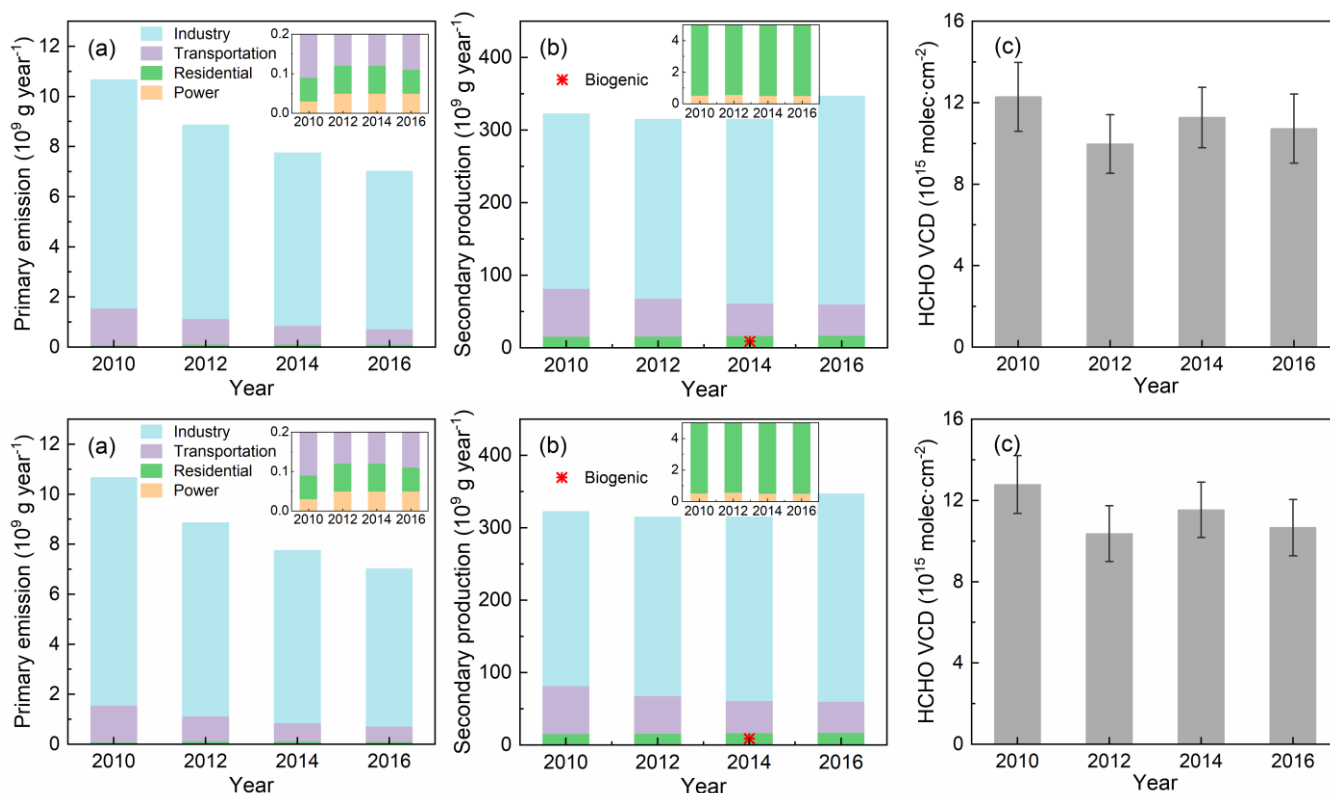
185　condition (Table S1) (Shen et al., 2019).

Figure 4. Primary and estimated secondary production of HCHO from anthropogenic NMVOCs, biogenic contribution of HCHO
190 **in 2014 was marked as red cross in Figure 4(b).**

In Fig. 4a and 4b, for the total of primary emissions and secondary productions, the contribution of industrial sector was much higher than other sectors, accounting for about 79.3% of the total, followed by transportation sector, accounting for about 15.7%. Residential and power sectors were far lower, the proportions over these years were basically less than 5%. As
195 major sectors, the contribution of industrial increased 17.2%, while the contribution of transportation decreased about 35.2%. The primary emission of HCHO keeps decreasing (about 34.2% compared to 2010), while secondary produced HCHO did not change significantly. Furthermore, the changes and proportional relationships between primary emission and secondary production of HCHO for these sectors are different, which means the VOCs source profile of different emission sectors would affect the amount of secondary HCHO production. It should be noted that the estimation here is the potential of
200 secondary HCHO production from anthropogenic NMVOCs, and does not represent the actually produced in the atmosphere. In addition, HCHO produced by biogenic sources in 2014 was also calculated, and the BVOCs emissions were referred from Liu et al. (Liu et al., 2018b; 2018c). HCHO yield from BVOCs emission was about 9.07×10^9 g, which is much smaller compared with anthropogenic contribution, indicating that the anthropogenic is the main contributor of secondary production

of HCHO in Shanghai (Shen et al., 2019; Fan et al., 2021). The spatial distribution of surface land types in Shanghai (Fig. S3) also suggest the less emission and contribution of biogenic sources in urbanized and densely populated area compared to forested regions.

Fig. 4c shows that the annual trend of HCHO VCDs is not synchronized with that of primary or secondary HCHO. It means that, besides the combined effect of the primary and secondary source, the changes of HCHO VCDs should also be affected complexly by various factors. In addition, it should be noted that HCHO yield from VOCs is proportional to NO_x condition (Palmer et al., 2006; Marais et al., 2012; Miller et al., 2017). With context of the continuous NO_x decreases in Shanghai, the estimation using a fixed HCHO yield may overestimate secondary HCHO production in later years (Xue et al., 2020). However, the NO_x concentration in Shanghai (basically 30-60 ppbv in urban) is still much higher than the defined high NO_x condition (1 ppbv) in previous studies (Gao et al., 2017). Therefore, in such a high NO_x condition, the effect of NO_x decreases on HCHO yield needs to be further studied.

3.3. FNR and O_3 formation regime

As the important precursors of O_3, HCHO and NO_2 can be served as indicators for VOCs and NO_x. On this basis, the HCHO/NO_2 ratio from satellite observation (FNR_{SAT}) can be employed to identify the O_3 formation regime. The variations of monthly averaged VCDs of HCHO, NO_2, and FNR_{SAT} in Shanghai over the past 10 years are given in Fig. 5. NO_2 VCDs were featured by the highest in winter and the lowest in summer, which was opposite to HCHO and fluctuated more fiercely. The peaks were mainly on account of its longer lifetime in winter (Zhang et al., 2007). While in summer, the adequate sunlight and precipitation accelerated the photochemical removal and wet deposition of NO_2, resulting in the dip (Wang et al., 2018; Xue et al., 2020). FNR_{SAT} also exhibited the obvious annual cycle of high in summer and low in winter. According to the criteria proposed by Duncan et al. (2010), O_3 formation regime in Shanghai was usually under NO_x-limited from June to August, and controlled by VOC-limited and transition regime for the rest of months. From May to September in 2014, Shanghai all under NO_x-limited regime, and FNR_{SAT} reached the highest value over the past 10 years. In 2019, the value of monthly FNR_{SAT} fluctuated gently, which showed the trend moving towards the transition regime threshold of 1-2.
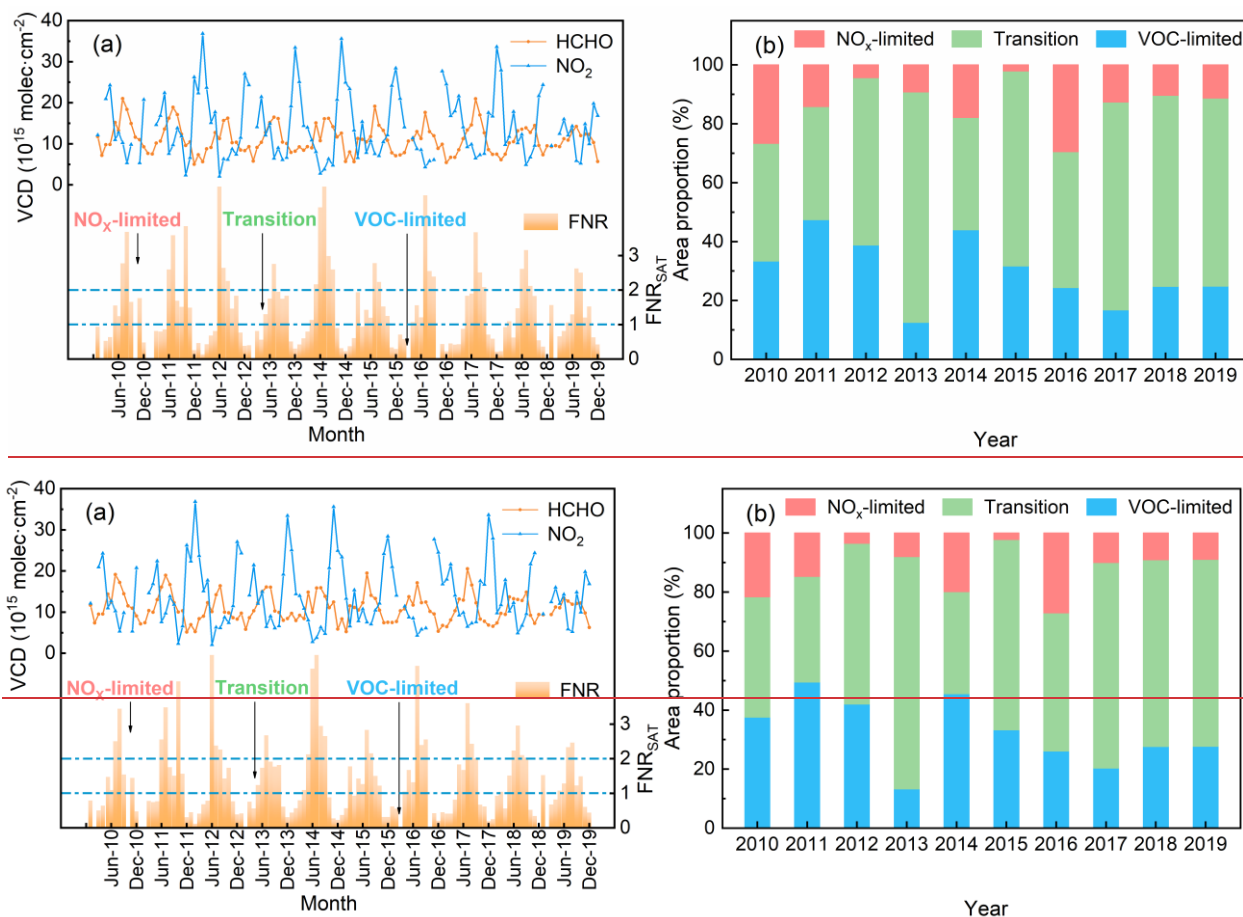
Figure 5. Temporal and spatial variation of FNR_{SAT} in Shanghai: (a) variations of HCHO, NO_2 and FNR_{SAT} from 2010 to 2019,
and (b) the area proportion for different O_3 formation regimes in these years.

The spatial distribution of FNR_{SAT} in Shanghai is presented in Fig. 6. Comparing FNR_{SAT} in 2019 with that in 2010, the NO_x-limited regime in the western Shanghai transformed into transition regime, and VOC-limited regime in the northern Chongming Island almost completely became transition regime. It manifests itself in the reduction in the NO_x-limited and VOC-limited regimes while the increase in the transition regime. Referring to previous study on the variation of NO_2 VCDs spatial distribution in Shanghai observed by satellite, this phenomenon may be related to the spatial characteristics of concentration variations of two precursors (Xue et al., 2020). This result is also reflected in Fig. 5b. In the past 10 years, the proportion decreased from 3~~37~~.~~46~~% to 2~~47~~.~~97~~% for VOC-limited area, and from 2~~61~~.~~76~~% to 1~~18~~.~~39~~% for NO_x-limited area, respectively. Meanwhile, the transition regime area increased from 40.~~0~~.~~8~~% to 63.~~83~~%. Xu et al. (2019) suggested that O_3 formation regime in Shanghai trend to transform from VOC-limited regime to NO_x-limited regime after 2020 through WRF-Chem model simulation. In this study, the increase of transition regime may be the transition state from VOC-limited to NO_x-limited regime.
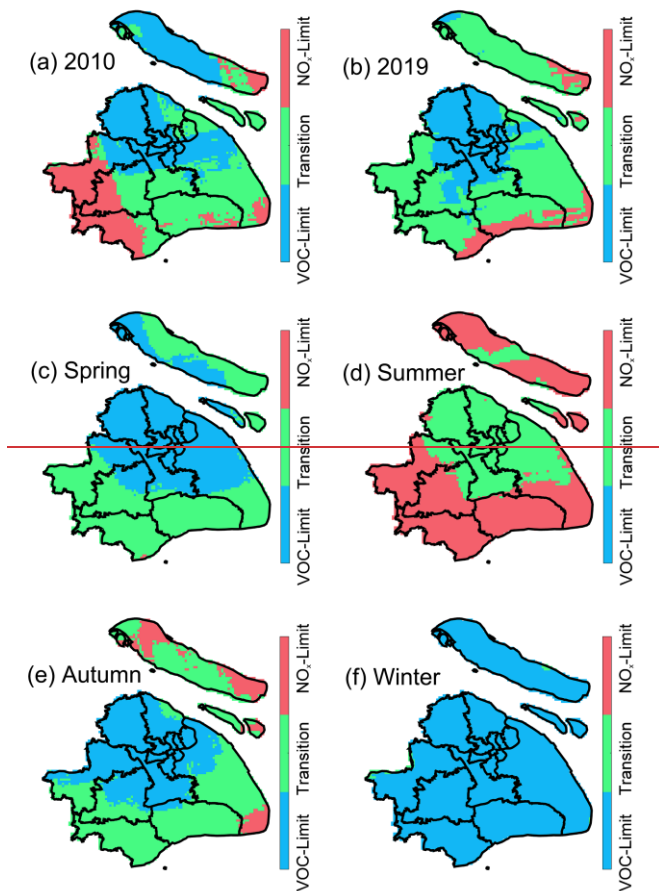
12
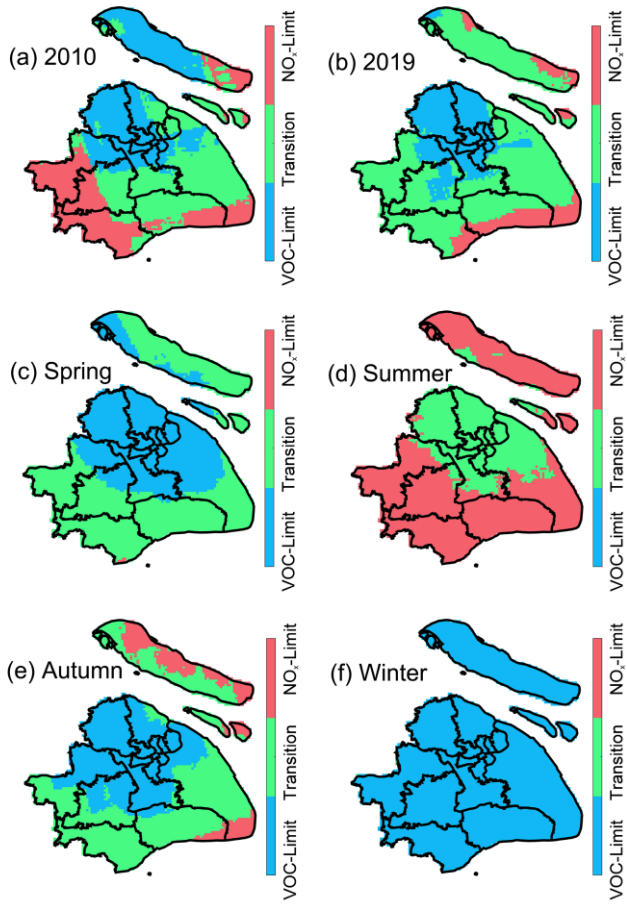
Figure 6. The spatial distribution of FNR$_{SAT}$ for (a) 2010, (b) 2019, and (c) to (f) different seasons in Shanghai.

245   Figure. 6c to Fig. 6f show the spatial distribution of FNR$_{SAT}$ for different seasons during the decade. In spring, the northern area of Shanghai was VOC-limited regime while the southern area was transition regime. From spring to summer, the VOC-limited area almost transformed into transition regime, and the transition regime nearly turned into NO$_x$-limited at the same time, which mainly caused by the increase of HCHO and the decrease of NO$_2$. The distribution in autumn was similar to that in spring. In winter, Shanghai was basically under VOC-limited. In the light of the temporal and spatial distribution of O$_3$

250   formation regime inferred by FNR$_{SAT}$, the emission reduction measures for O$_3$ precursors would be more rationally.

Besides, there are differences in O$_3$ formation regime in urban and suburban areas of Shanghai, with the main manifestation that the central urban area was inclined to be in VOC-limited regime and the suburban area was more likely to be in NO$_x$-limited regime. In order to analyse the differences in more detail, area within 10 km around the Jiangwan campus of Fudan University was selected to represent the urban area (about 12 km to the city center), and equally sized area around Dianshan

255   Lake (31.09°N, 120.98°E) of Qingpu district was regarded as the suburban area (about 50 km to the city center), respectively. Since O$_3$ pollution is relatively serious from April to September, this period can be chosen as a research case. The maximum 8-hour average concentration of O$_3$ at the Hongkou and the Qingpu Dianshan Lake Site were used to characterize O$_3$

14

concentration in urban and suburban areas. NO$_2$ VCDs in urban area were higher than that in suburban, while HCHO VCDs presented the opposite character (Fig. 7a). The lower NO$_2$ in suburban area was associated with the less NO$_x$ emission than that in urban, corresponding to the larger FNR$_{SAT}$. From Fig. 7b, the O$_3$ production was under transition regime in ~~sub~~urban area ~~except for 2016~~, while ~~VOC~~NO$_x$-limited regime occupied for most years in ~~urban~~ suburban area. The O$_3$ concentration in suburban area was always higher than that in urban (Fig. 7c). In this study, ~~transition regime in suburban for most years led to higher O$_3$ concentration correspondingly (Jin et al., 2020). In addition,~~ high concentration of NO$_x$ in urban area may lead to titration of O$_3$ by NO, which would ~~also~~ cause the lower O$_3$ concentration in urban (Geng et al., 2008; Duncan et al., 2010).
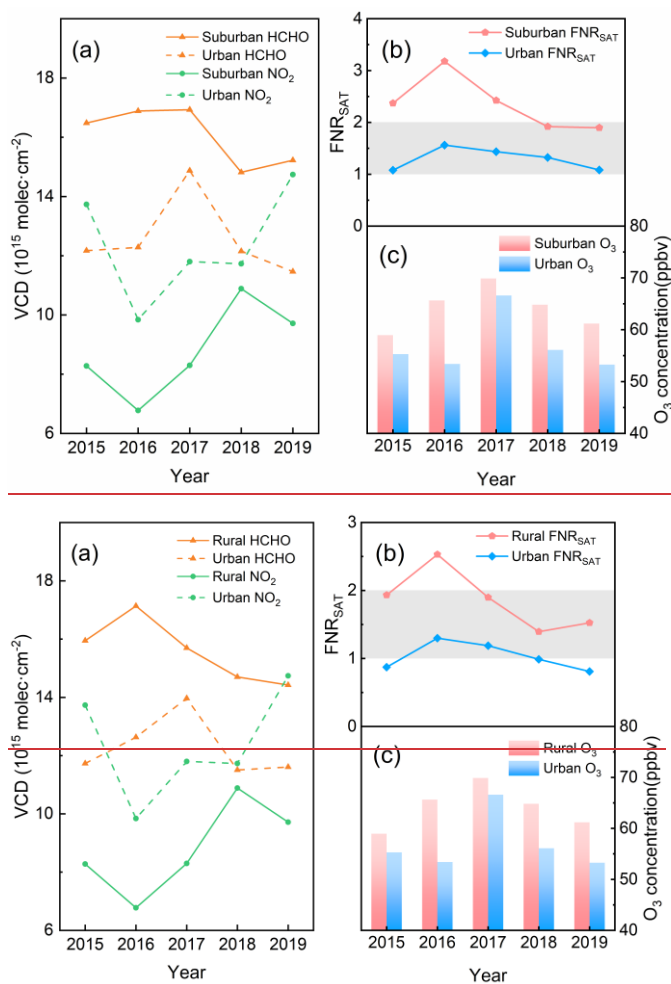

Figure 7. Differences of (a) satellite observation of HCHO and NO$_2$ VCDs, (b) FNR$_{SAT}$ and (c) surface O$_3$ concentration in urban and suburban areas of Shanghai from 2015 to 2019.

15

3.4. Correction of FNR$_{SAT}$

FNR is originally proposed as an indicator to characterize the sensitivity of the instantaneous O$_3$ production rate (Duncan et al., 2010). Satellite observation only reflects the averaged column of the trace gases around overpass time, so the FNR$_{SAT}$ may not accurately infer the surface O$_3$ formation regime during the day (Duncan et al., 2010; Jin and Holloway, 2015; Jin et al., 2017). FNR$_{SAT}$ was compared with FNR$_{LP}$ at the satellite overpass time on the monthly and daily scales. Results show that FNR$_{SAT}$ and FNR$_{LP}$ were consistent well on monthly scale (R^2=0.95, between April and August), but they were quite different on the daily scale, and the relationship was easily affected by the boundary layer height (BLH) and other factors (Schroeder et al., 2017).

As shown in Fig. 8a to Fig.8c, LP-DOAS observation provided FNR$_{LP}$ with the high temporal resolution throughout the day, and FNR$_{LP}$ was in good agreement with hourly O$_3$ concentration. It means that FNR$_{LP}$ should be a good indicator to distinguish the formation regime of surface O$_3$ on a detailed time scale. In addition, the highest value of FNR$_{LP}$ at noon means that FNR$_{SAT}$ at overpass time approximately close to the highest level in a day. Thus, it would be valuable to introduce the time series of FNR$_{LP}$ to make FNR$_{SAT}$ better reflect the characteristic of O$_3$ formation during the daytime.
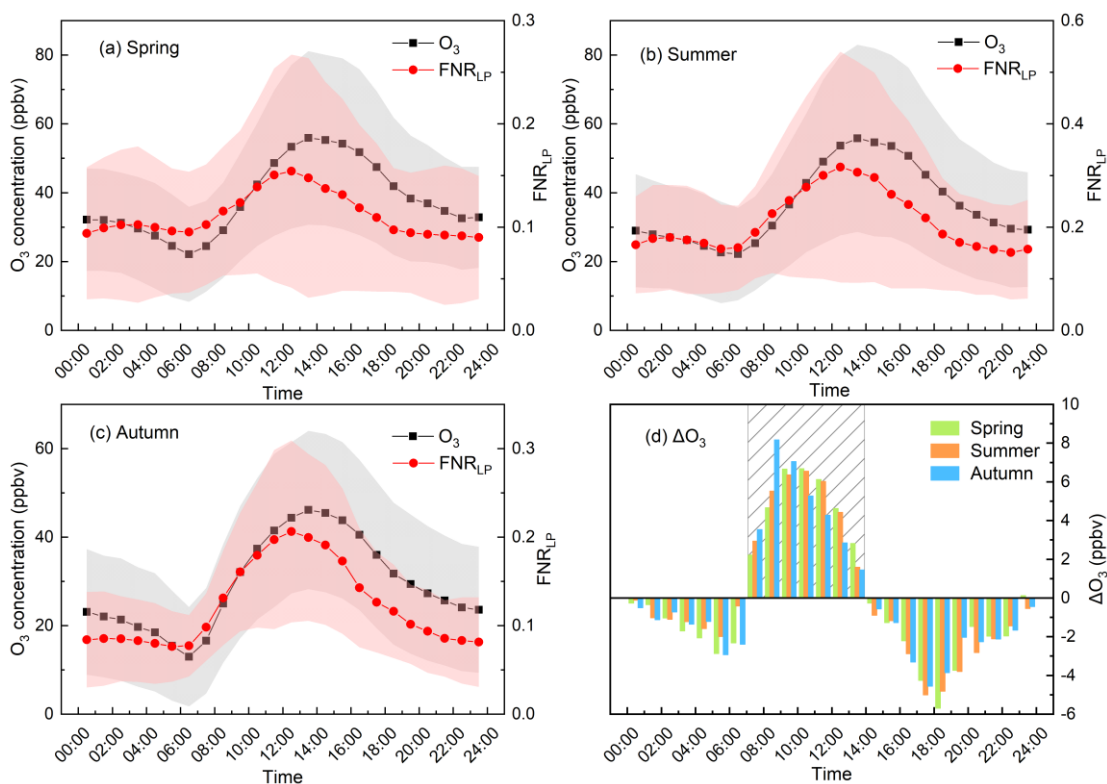
Figure 8. Diurnal variations of FNR$_{LP}$, O$_3$ and ΔO$_3$ for spring, summer and autumn during 2018-2019. ΔO$_3$ represents increment of hourly O$_3$ concentration, as referred to Eq. (3). The shaded area in (d) represents the period when ΔO$_3$ greater than 0.

16

Three cases during the LP-DOAS observation at the Jiangwan campus of Fudan University were selected for the further discussion under the criteria of the hourly concentration of O_3 exceeding 200 μg/m^3 (secondary concentration limit stipulated in ambient air quality standards of China, GB 3095-2012). In Fig. 9a and Fig. 9c, the upward trend in FNR_{LP} as the O_3 concentration increases means that the formation of O_3 was under VOC-limited regime in Case 1 and 3. VOC-limited and transition regimes caught in Case 1 through FNR_{SAT} were different from that identified by FNR_{LP}. In Case 3, the O_3 formation regime remained in VOC-limited regime, which was the same as FNR_{LP}. As shown in Fig. 8b, FNR_{LP} indicated that the O_3 formation regime switched between three regimes in Case 2. As O_3 concentration increasing, the growth of FNR_{LP} at beginning indicated VOC-limited regime, while the subsequent slow variation suggested transition regime. When O_3 concentration reached maximum, FNR_{LP} got smaller, which referred to NO_x-limited regime. But FNR_{SAT} only captured the VOC-limited and transition regime in Case 2. According to the results above, it is feasible and necessary to correct FNR_{SAT} to better represent the sensitivity of surface O_3 formation. Due to the less O_3 pollution in winter, FNR_{SAT} was only corrected for the remaining three seasons.
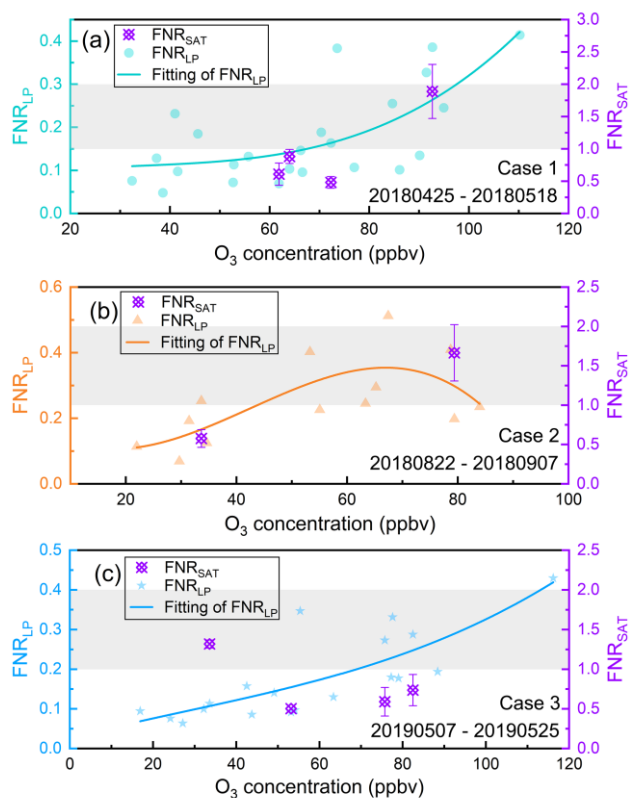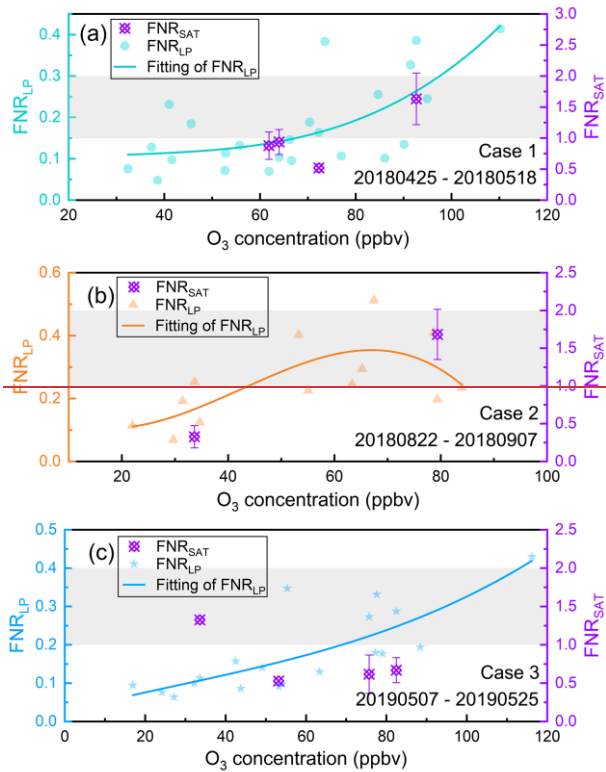
Figure 9. Comparison of FNR$_{SAT}$ and FNR$_{LP}$ in three O$_3$ pollution cases. The curves are polynomial fit of FNR$_{LP}$, and the points are FNR$_{SAT}$ in corresponding cases, the gray area indicates the transition regime for FNR$_{SAT}$. Only LP-DOAS measured data between 08:00-18:00 LT were contained.

The correction of FNR$_{SAT}$ was achieved through the following process. Firstly, the ratio of FNR at satellite overpass time to averaged FNR during O$_3$ pollution period (ΔO_3 greater than 0, i.e. 07:00 to 13:00 LT, referred to Fig. 8d) obtained from ground surface measurement was assumed to be same with that of satellite observation, which is expressed as:

$$\frac{FNR_{SAT}}{\overline{FNR}_{SAT}} = \frac{FNR_{LP,overpass\ time}}{\overline{FNR}_{LP}} \tag{1}$$

where $\overline{FNR}_{LP}$ is weighted average of FNR during O$_3$ pollution period observed by ground surface LP-DOAS measurement, FNR$_{LP,overpass\ time}$ is ground surface FNR observed at satellite overpass time. $\frac{FNR_{LP,overpass\ time}}{\overline{FNR}_{LP}}$ reflects the numerical relationship of FNR between satellite overpassed time and O$_3$ polluted period during a day, and can be serve as the correction coefficient to realize the correction for FNR$_{SAT}$ on time scale to obtain the $\overline{FNR}_{SAT}$. Considering the relationship between time series of FNR and O$_3$ formation, ΔO_3 was involved to calculate the weighted average of FNR$_{LP}$ ($\overline{FNR}_{LP}$) during 07:00 to 13:00 LT via Eq. (2), which can better indicate the ozone formation in a day.

$$\overline{FNR}_{LP} = \frac{\sum_{T=7}^{13} FNR_{LP,T} \times \Delta\Omega_{O3,T}}{\sum_{T=7}^{13} \Delta\Omega_{O3,T}} \tag{2}$$

18

$$\Delta\Omega_{O3,T} = \Omega_{O3,T} - \Omega_{O3,T-1} \qquad (3)$$

Where $\Delta\Omega_{O3,T}$ is the increase of O_3 concentration at time T, $FNR_{LP,T}$ is the FNR_{LP} at time T. Moreover, variation characteristics of FNR_{LP} in different seasons (as shown in Fig. 8a to Fig. 8c) suggest that the correction of FNR_{SAT} should be discussed seasonally.

320 Afterwards, the seasonal correction coefficients of 0.85, 0.84, and 0.77 were obtained for spring, summer, and autumn, respectively. It is noted that all the correct coefficients were less than 1 due to the FNR_{LP} value for OMI overpasses time relatively larger than other time. It would inevitably make the O_3 formation regime inferred by corrected FNR_{SAT} trend to be VOC-limited. There were 87 months with effective FNR_{SAT} in three seasons during 2010-2019 and the proportion of months for different regimes was listed in Table 1. Before the correction, the VOC-limited and NO_x-limited regimes, as well as

325 transition regime were almost accounted for about one-third of the total months. After the correction, both of months for VOC-limited and transition regimes increased. The months under VOC-limited regime increased by 21.4~~5~~% particularly, while decreased about ~~3~~25.1~~9~~% for NO_x-limited regime. Jin et al. (2020) used O_3 exceedance probability as the indicator to analyse non-linear dependence of long-term surface O_3 concentration on precursor emissions, and determined the OMI HCHO/NO_2 under transition regime ranging from 3.2 to 4.1. These thresholds are significantly larger than the value

330 proposed by Duncan et al. (2010), which has the equivalent effect as the use of correction factors less than 1 in this study.

Table 1. Variations in the number and proportions of months in 2010-2019 for each regime before and after the correction.

| Regime	Before corrected	Percentage before corrected	After corrected	Percentage after corrected	Percentage of change
VOC-limited	28	32.2%	34~~5~~	39.1~~40.2~~%	21.4~~5.40~~%
Transition	32~~1~~	36.6~~5.68~~%	33	37.9%	36.1~~5~~%
NO_x-limited	27~~8~~	31.0~~2.2~~%	20~~19~~	23.1~~.08~~%	-25.9~~32.91~~%

In terms of spatial distribution, the O_3 formation regime after correction in different seasons is shown in Fig. 10. Compared with Fig. 6, part of the transition regime area in spring transformed into VOC-limited regime after the correction, VOC-

335 limited regime obviously expanded and increased about 18~~5.26~~%. Most area in Chongming Island transformed into VOC-limited regime. In summer, part of the NO_x-limited regime area transformed into transition regime, and the area of transition regime increased about 16~~1.29~~%. In autumn, the NO_x-limited regime almost disappeared, and the proportion of the transition regime area also decreased significantly, for about 10~~3.42~~%, while the proportion of the VOC-limited regime area increased about 21.5~~2~~%. The O_3 formation regime in Chongming Island was basically under transition regime. Researchers also

340 pointed that thresholds of criteria would be regionally dependent, so the local surface FNR and O_3 concentration should be introduced in satellite correction (Duncan et al., 2010; Jin et al., 2020).
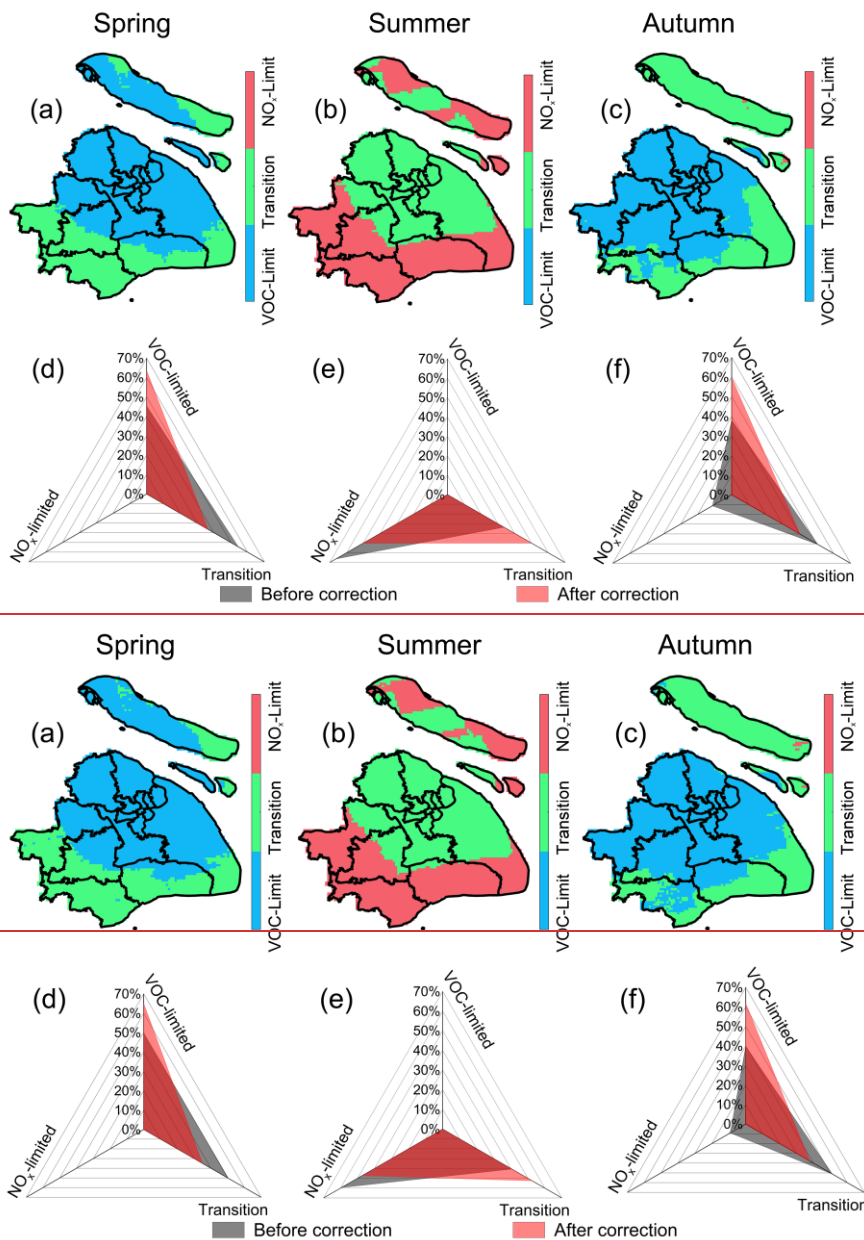
Figure 10. Spatial distribution of O₃ formation regime (upper row) and area proportion for each regime (bottom row) after correction for different seasons in Shanghai during 2010-2019.

In order to verify whether the correction of the satellite FNR improved the regime classification, O₃ formation regimes determined by satellite FNR before and after the correction were compared with that of surface observation. The variations of O₃ with surface HCHO and NO₂ have been plotted to determine the O₃ formation regimes from the surface observation

350 (Figure 11). The daytime surface HCHO and NO_2 are from LP-DOAS measurements, and the O_3 observed by SP-DOAS (short-path DOAS), which is also located at Jiangwan campus of Fudan University, have been used with a high temporal resolution. O_3 formation regimes inferred from satellite FNR before and after the correction have also been marked in Figure 11 separately.
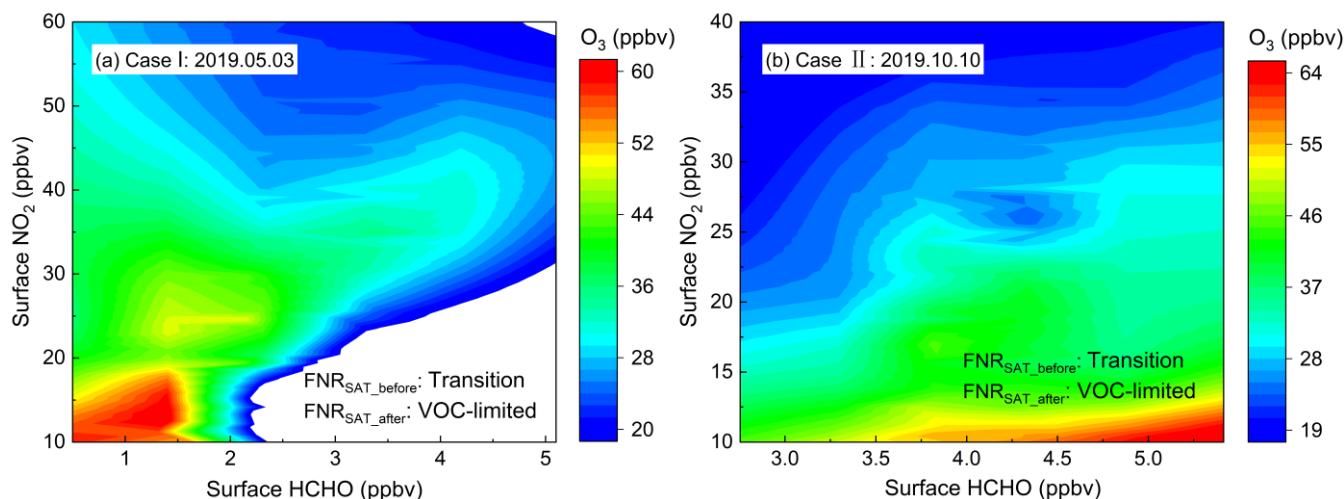
355

Figure 11. The variation of O_3 with surface HCHO and NO_2 for two cases of (a) May 3th, 2019 and (b) October 10th, 2019. FNR$_{SAT\_before}$ and FNR$_{SAT\_after}$ indicate the O_3 formation regimes inferred from the satellite FNR before and after the correction.

For Case I, O_3 decreases with the increase of NO_2, which can be attributed to the titration of O_3 by NO (Duncan et al., 2010).
360 O_3 increased from top to bottom indicating it was under VOC-limited regime in Case I (Luo et al., 2020). For Case II, it can be seen that the high O_3 appeared with high HCHO and low NO_2, indicating it was under VOC-limited regime. The uncorrected satellite FNR indicated that these two cases were both under transition regime, while the corrected satellite FNR indicated they transferred to VOC-limited regime, which are consistent with the results of surface observation. It indicates that the correction of FNR$_{SAT}$ in this study can be considered to be effective and make sense.

4. Summary and conclusions

Satellite data of OMI were used to study the temporal and spatial variation of HCHO in Shanghai from 2010 to 2019. HCHO VCDs fluctuated during the 10 years with obvious seasonal characteristics of highest value in summer, the lowest value in winter, and the moderate level in spring and autumn. In terms of spatial distribution, HCHO VCDs in western area were much higher than that in eastern coastal area. Compared with 2010, HCHO VCDs of Shanghai in 2019 showed an overall
370 downward trend. As for the influencing factors, temperature give the significant positive effect on HCHO VCDs while the

21

abundant precipitation reduces HCHO in summer. Industry was an important contributor of HCHO, and anthropogenic secondary production of HCHO occupied the main part of the HCHO source.

In the past 10 years, O_3 formation regime changed toward transition regime gradually. O_3 formation regime in urban area was more likely to be VOC-limited regime, while regime in suburban area was more likely to be NO_x-limited. FNR_{SAT} was corrected based on the hourly surface FNR and O_3 data to make it better to reflect O_3 formation in a day. After correcting FNR_{SAT} with seasonal correction coefficients of 0.85, 0.84, and 0.77 for spring, summer, and autumn respectively, O_3 formation regime in Shanghai was more inclined to VOC-limited in both time and spatial distribution, and the effectiveness of FNR_{SAT} correction was confirmed by the surface observation. Thus, this correction is significant for using satellite data to improve the accuracy in indicating surface O_3 formation.

References

An, J. Y., Huang, Y. W., Huang, C., Wang, X., Yan, R. S., Wang, Q., Wang, H. L., Jing, S. A., Zhang, Y., Liu, Y. M., Chen, Y., Xu, C., Qiao, L. P., Zhou, M., Zhu, S. H., Hu, Q. Y., Lu, J., and Chen, C. H.: Emission inventory of air pollutants and chemical speciation for specific anthropogenic sources based on local measurements in the Yangtze River Delta region, China, Atmos Chem Phys, 21, 2003-2025, https://doi.org/10.5194/acp-21-2003-2021, 2021.

Bovensmann, H., Burrows, J. P., Buchwitz, M., Frerick, J., Noel, S., Rozanov, V. V., Chance, K. V., and Goede, A. P. H.: SCIAMACHY: Mission objectives and measurement modes, J Atmos Sci, 56, 127-150, https://doi.org/Doi 10.1175/1520-0469(1999)056<0127:Smoamm>2.0.Co;2, 1999.

Burrows, J. P., Weber, M., Buchwitz, M., Rozanov, V., Ladstatter-Weissenmayer, A., Richter, A., DeBeek, R., Hoogen, R., Bramstedt, K., Eichmann, K. U., and Eisinger, M.: The global ozone monitoring experiment (GOME): Mission concept

and first scientific results, J Atmos Sci, 56, 151-175, https://doi.org/Doi 10.1175/1520-0469(1999)056<0151:Tgomeg>2.0.Co;2, 1999.

Callies, J., Corpaccioli, E., Eisinger, M., Hahne, A., and Lefebvre, A.: GOME-2 - Metop's second-generation sensor for operational ozone monitoring, Esa Bull-Eur Space, 28-36, 2000.

410 Chan, K. L., Wang, Z. R., Ding, A. J., Heue, K. P., Shen, Y. C., Wang, J., Zhang, F., Shi, Y. N., Hao, N., and Wenig, M.: MAX-DOAS measurements of tropospheric NO_2 and HCHO in Nanjing and a comparison to ozone monitoring instrument observations, Atmos Chem Phys, 19, 10051-10071, https://doi.org/10.5194/acp-19-10051-2019, 2019.

De Smedt, I., Van Roozendael, M., Stavrakou, T., Muller, J. F., Lerot, C., Theys, N., Valks, P., Hao, N., and van der A, R.: Improved retrieval of global tropospheric formaldehyde columns from GOME-2/MetOp-A addressing noise reduction
415 and instrumental degradation issues, Atmos Meas Tech, 5, 2933-2949, https://doi.org/10.5194/amt-5-2933-2012, 2012.

Duncan, B. N., Yoshida, Y., Damon, M. R., Douglass, A. R., and Witte, J. C.: Temperature dependence of factors controlling isoprene emissions, Geophys Res Lett, 36, https://doi.org/10.1029/2008GL037090, 2009.

Duncan, B. N., Yoshida, Y., Olson, J. R., Sillman, S., Martin, R. V., Lamsal, L., Hu, Y. T., Pickering, K. E., Retscher, C., Allen, D. J., and Crawford, J. H.: Application of OMI observations to a space-based indicator of NO_x and VOC controls
420 on surface ozone formation, Atmos Environ, 44, 2213-2223, https://doi.org/10.1016/j.atmosenv.2010.03.010, 2010.

Fan, J. C., Ju, T. Z., Wang, Q. H., Gao, H. Y., Huang, R. R., and Duan, J. L.: Spatiotemporal variations and potential sources of tropospheric formaldehyde over eastern China based on OMI satellite data, Atmos Pollut Res, 12, 272-285, https://doi.org/10.1016/j.apr.2020.09.011, 2021.

Fioletov, V. E., McLinden, C. A., Krotkov, N., Moran, M. D., and Yang, K.: Estimation of SO_2 emissions using OMI
425 retrievals, Geophys Res Lett, 38, 5, https://doi.org/10.1029/2011gl049402, 2011.

Gao, W., Tie, X. X., Xu, J. M., Huang, R. J., Mao, X. Q., Zhou, G. Q., and Chang, L. Y.: Long-term trend of O_3 in a mega City (Shanghai), China: Characteristics, causes, and interactions with precursors, Sci Total Environ, 603, 425-433, https://doi.org/10.1016/j.scitotenv.2017.06.099, 2017.

Geng, F. H., Tie, X. X., Xu, J. M., Zhou, G. Q., Peng, L., Gao, W., Tang, X., and Zhao, C. S.: Characterizations of ozone,
430 NO_x, and VOCs measured in Shanghai, China, Atmos Environ, 42, 6873-6883, https://doi.org/10.1016/j.atmosenv.2008.05.045, 2008.

Jin, X. M., and Holloway, T.: Spatial and temporal variability of ozone sensitivity over China observed from the Ozone Monitoring Instrument, J. Geophys. Res.-Atmos., 120, 7229-7246, https://doi.org/10.1002/2015jd023250, 2015.

Jin, X. M., Fiore, A. M., Murray, L. T., Valin, L. C., Lamsal, L. N., Duncan, B., Folkert Boersma, K., De Smedt, I., Abad, G.
435 G., Chance, K., and Tonnesen, G. S.: Evaluating a Space-Based Indicator of Surface Ozone-NO_x-VOC Sensitivity Over Midlatitude Source Regions and Application to Decadal Trends, J. Geophys. Res.-Atmos., 122, 10231-10253, https://doi.org/10.1002/2017jd026720, 2017.

Jin, X. M., Fiore, A., Boersma, K. F., De Smedt, I., and Valin, L.: Inferring Changes in Summertime Surface Ozone-NO_x-VOC Chemistry over US Urban Areas from Two Decades of Satellite and Ground-Based Observations, Environ Sci
440 Technol, 54, 6518-6529, https://doi.org/10.1021/acs.est.9b07785, 2020.

Krotkov, N. A., McLinden, C. A., Li, C., Lamsal, L. N., Celarier, E. A., Marchenko, S. V., Swartz, W. H., Bucsela, E. J., Joiner, J., Duncan, B. N., Boersma, K. F., Veefkind, J. P., Levelt, P. F., Fioletov, V. E., Dickerson, R. R., He, H., Lu, Z. F., and Streets, D. G.: Aura OMI observations of regional SO_2 and NO_2 pollution changes from 2005 to 2015, Atmos Chem Phys, 16, 4605-4629, https://doi.org/10.5194/acp-16-4605-2016, 2016.

445 Lee, H., Ryu, J., Irie, H., Jang, S. H., Park, J., Choi, W., and Hong, H.: Investigations of the Diurnal Variation of Vertical HCHO Profiles Based on MAX-DOAS Measurements in Beijing: Comparisons with OMI Vertical Column Data, Atmosphere-Basel, 6, 1816-1832, https://doi.org/10.3390/atmos6111816, 2015.

Levelt, P. F., Van den Oord, G. H. J., Dobber, M. R., Malkki, A., Visser, H., de Vries, J., Stammes, P., Lundell, J. O. V., and Saari, H.: The Ozone Monitoring Instrument, Ieee T Geosci Remote, 44, 1093-1101,
450 https://doi.org/10.1109/Tgrs.2006.872333, 2006.

Li, K., Jacob, D. J., Liao, H., Shen, L., Zhang, Q., and Bates, K. H.: Anthropogenic drivers of 2013-2017 trends in summer surface ozone in China, P Natl Acad Sci USA, 116, 422-427, https://doi.org/10.1073/pnas.1812168116, 2019.

Li, X., Rohrer, F., Brauers, T., Hofzumahaus, A., Lu, K., Shao, M., Zhang, Y. H., and Wahner, A.: Modeling of HCHO and CHOCHO at a semi-rural site in southern China during the PRIDE-PRD2006 campaign, Atmos Chem Phys, 14, 12291-
455 12305, https://doi.org/10.5194/acp-14-12291-2014, 2014.

Ling, Z. H., Guo, H., Chen, G. X., Lam, S. H. M., and Fan, S. J.: Formaldehyde and Acetaldehyde at Different Elevations in Mountainous Areas in Hong Kong, Aerosol Air Qual Res, 16, 1868-1878, https://doi.org/10.4209/aaqr.2015.09.0571, 2016.

Liu, H. R., Liu, C., Xie, Z. Q., Li, Y., Huang, X., Wang, S. S., Xu, J., and Xie, P. H.: A paradox for air pollution controlling in China revealed by "APEC Blue" and "Parade Blue", Sci Rep-Uk, 6, 13, https://doi.org/10.1038/srep34408, 2016.

Liu, R., Feng, T., Wang, S. S., Shi, C. Z., Guo, Y. L., Nan, J. L., Deng, Y., and Zhou, B.: OMI satellite observed formaldehyde column from 2006 to 2015 over Xishuangbanna, southwest China, and validation using ground based zenith-sky DOAS, Sci Total Environ, 613, 168-175, https://doi.org/10.1016/j.scitotenv.2017.08.210, 2018a.

Liu, Y., Li, L., An, J., Zhang, W., Yan, R., Huang, L., Huang, C., Wang, H., Wang, Q., and Wang, M.: Emissions, Chemical Composition, and Spatial and Temporal Allocation of the BVOCs in the Yangtze River Delta Region in 2014, ENVIRONMENTAL SCIENCE, 39, 608-617, 2018b.

Liu, Y., Li, L., An, J. Y., Huang, L., Yan, R. S., Huang, C., Wang, H. L., Wang, Q., Wang, M., and Zhang, W.: Estimation of biogenic VOC emissions and its impact on ozone formation over the Yangtze River Delta region, China, Atmos Environ, 186, 113-128, https://doi.org/10.1016/j.atmosenv.2018.05.027, 2018c.

Liu, Y., Tang, Z. P., Abera, T., Zhang, X. Z., Hakola, H., Pellikka, P., and Maeda, E.: Spatio-temporal distribution and source partitioning of formaldehyde over Ethiopia and Kenya, Atmos Environ, 237, 9, https://doi.org/10.1016/j.atmosenv.2020.117706, 2020.

Luo, H. H., Yang, L. F., Yuan, Z. B., Zhao, K. H., Zhang, S., Duan, Y. S., Huang, R. Z., and Fu, Q. Y.: Synoptic condition-driven summertime ozone formation regime in Shanghai and the implication for dynamic ozone control strategies, Sci Total Environ, 745, 12, https://doi.org/10.1016/j.scitotenv.2020.141130, 2020.

Marais, E. A., Jacob, D. J., Kurosu, T. P., Chance, K., Murphy, J. G., Reeves, C., Mills, G., Casadio, S., Millet, D. B., Barkley, M. P., Paulot, F., and Mao, J.: Isoprene emissions in Africa inferred from OMI observations of formaldehyde columns, Atmos Chem Phys, 12, 6219-6235, https://doi.org/10.5194/acp-12-6219-2012, 2012.

Martin, R. V., Fiore, A. M., and Van Donkelaar, A.: Space-based diagnosis of surface ozone sensitivity to anthropogenic emissions, Geophys Res Lett, 31, L06120 06121-06124, https://doi.org/10.1029/2004gl019416, 2004a.

Martin, R. V., Parrish, D. D., Ryerson, T. B., Nicks, D. K., Chance, K., Kurosu, T. P., Jacob, D. J., Sturges, E. D., Fried, A., and Wert, B. P.: Evaluation of GOME satellite measurements of tropospheric NO$_2$ and HCHO using regional data from aircraft campaigns in the southeastern United States, J. Geophys. Res.-Atmos., 109, 11, https://doi.org/10.1029/2004jd004869, 2004b.

McLinden, C. A., Fioletov, V., Boersma, K. F., Krotkov, N., Sioris, C. E., Veefkind, J. P., and Yang, K.: Air quality over the Canadian oil sands: A first assessment using satellite observations, Geophys Res Lett, 39, 8, https://doi.org/10.1029/2011gl050273, 2012.

Miller, C. C., Jacob, D. J., Marais, E. A., Yu, K. R., Travis, K. R., Kim, P. S., Fisher, J. A., Zhu, L., Wolfe, G. M., Hanisco, T. F., Keutsch, F. N., Kaiser, J., Min, K. E., Brown, S. S., Washenfelder, R. A., Abad, G. G., and Chance, K.: Glyoxal yield from isoprene oxidation and relation to formaldehyde: chemical mechanism, constraints from SENEX aircraft observations, and interpretation of OMI satellite data, Atmos Chem Phys, 17, 8725-8738, https://doi.org/10.5194/acp-17-8725-2017, 2017.

Millet, D. B., Jacob, D. J., Boersma, K. F., Fu, T. M., Kurosu, T. P., Chance, K., Heald, C. L., and Guenther, A.: Spatial distribution of isoprene emissions from North America derived from formaldehyde column measurements by the OMI satellite sensor, J. Geophys. Res.-Atmos., 113, 18, https://doi.org/10.1029/2007jd008950, 2008.

Narumi, D., Kondo, A., and Shimoda, Y.: The effect of the increase in urban temperature on the concentration of photochemical oxidants, Atmos Environ, 43, 2348-2359, https://doi.org/10.1016/j.atmosenv.2009.01.028, 2009.

Palmer, P. I., Abbot, D. S., Fu, T. M., Jacob, D. J., Chance, K., Kurosu, T. P., Guenther, A., Wiedinmyer, C., Stanton, J. C., Pilling, M. J., Pressley, S. N., Lamb, B., and Sumner, A. L.: Quantifying the seasonal and interannual variability of North American isoprene emissions using satellite observations of the formaldehyde column, J. Geophys. Res.-Atmos., 111, 14, https://doi.org/10.1029/2005jd006689, 2006.

Pang, X. B., Mu, Y. J., Lee, X. Q., Zhang, Y. J., and Xu, Z.: Influences of characteristic meteorological conditions on atmospheric carbonyls in Beijing, China, Atmos Res, 93, 913-919, https://doi.org/10.1016/j.atmosres.2009.05.001, 2009.

Schroeder, J. R., Crawford, J. H., Fried, A., Walega, J., Weinheimer, A., Wisthaler, A., Muller, M., Mikoviny, T., Chen, G.,
505   Shook, M., Blake, D. R., and Tonnesen, G. S.: New insights into the column CH_2O/NO_2 ratio as an indicator of near-surface ozone sensitivity, J. Geophys. Res.-Atmos., 122, 8885-8907, https://doi.org/10.1002/2017jd026781, 2017.

Sharkey, T. D., and Loreto, F.: Water-stress, temperature, and light effects on the capacity for isoprene emission and photosynthesis of kudzu leaves, Oecologia, 95, 328-333, https://doi.org/10.1007/bf00320984, 1993.

Shen, L., Jacob, D. J., Zhu, L., Zhang, Q., Zheng, B., Sulprizio, M. P., Li, K., De Smedt, I., Abad, G. G., Cao, H. S., Fu, T.
510   M., and Liao, H.: The 2005-2016 Trends of Formaldehyde Columns Over China Observed by Satellites: Increasing Anthropogenic Emissions of Volatile Organic Compounds and Decreasing Agricultural Fire Emissions, Geophys Res Lett, 46, 4468-4475, https://doi.org/10.1029/2019gl082172, 2019.

Sillman, S.: The use of NO_y, H_2O_2, and HNO_3 as indicators for Ozone-NO_x-Hydrocarbon sensitivity in Urban Locations, J. Geophys. Res.-Atmos., 100, 14175-14188, https://doi.org/doi 10.1029/94jd02953, 1995.

515 Souri, A. H., Choi, Y., Jeon, W., Woo, J. H., Zhang, Q., and Kurokawa, J.: Remote sensing evidence of decadal changes in major tropospheric ozone precursors over East Asia, J. Geophys. Res.-Atmos., 122, 2474-2492, https://doi.org/10.1002/2016jd025663, 2017.

Stavrakou, T., Muller, J. F., De Smedt, I., Van Roozendael, M., van der Werf, G. R., Giglio, L., and Guenther, A.: Global emissions of non-methane hydrocarbons deduced from SCIAMACHY formaldehyde columns through 2003-2006,
520   Atmos Chem Phys, 9, 3663-3679, https://doi.org/10.5194/acp-9-3663-2009, 2009.

Su, W. J., Liu, C., Hu, Q. H., Zhao, S. H., Sun, Y. W., Wang, W., Zhu, Y. Z., Liu, J. G., and Kim, J.: Primary and secondary sources of ambient formaldehyde in the Yangtze River Delta based on Ozone Mapping and Profiler Suite (OMPS) observations, Atmos Chem Phys, 19, 6717-6736, https://doi.org/10.5194/acp-19-6717-2019, 2019.

Veefkind, J. P., Aben, I., McMullan, K., Forster, H., de Vries, J., Otter, G., Claas, J., Eskes, H. J., de Haan, J. F., Kleipool,
525   Q., van Weele, M., Hasekamp, O., Hoogeveen, R., Landgraf, J., Snel, R., Tol, P., Ingmann, P., Voors, R., Kruizinga, B., Vink, R., Visser, H., and Levelt, P. F.: TROPOMI on the ESA Sentinel-5 Precursor: A GMES mission for global observations of the atmospheric composition for climate, air quality and ozone layer applications, Remote Sens Environ, 120, 70-83, https://doi.org/10.1016/j.rse.2011.09.027, 2012.

Vigouroux, C., Langerock, B., Aquino, C. A. B., Blumenstock, T., Cheng, Z. B., De Maziere, M., De Smedt, I., Grutter, M.,
530   Hannigan, J. W., Jones, N., Kivi, R., Loyola, D., Lutsch, E., Mahieu, E., Makarova, M., Metzger, J. M., Morino, I., Murata, I., Nagahama, T., Notholt, J., Ortega, I., Palm, M., Pinardi, G., Rohling, A., Smale, D., Stremme, W., Strong, K., Sussmann, R., Te, Y., van Roozendael, M., Wang, P. C., and Winkler, H.: TROPOMI-Sentinel-5 Precursor formaldehyde validation using an extensive network of ground-based Fourier-transform infrared stations, Atmos Meas Tech, 13, 3751-3767, https://doi.org/10.5194/amt-13-3751-2020, 2020.

535 Wang, T., Wang, P. C., Theys, N., Tong, D., Hendrick, F., Zhang, Q., and Van Roozendael, M.: Spatial and temporal changes in SO_2 regimes over China in the recent decade and the driving mechanism, Atmos Chem Phys, 18, 18063-18078, https://doi.org/10.5194/acp-18-18063-2018, 2018.

Wang, Y., Beirle, S., Lampel, J., Koukouli, M., De Smedt, I., Theys, N., Li, A., Wu, D. X., Xie, P. H., Liu, C., Van Roozendael, M., Stavrakou, T., Muller, J. F., and Wagner, T.: Validation of OMI, GOME-2A and GOME-2B
540   tropospheric NO_2, SO_2 and HCHO products using MAX-DOAS observations from 2011 to 2014 in Wuxi, China: investigation of the effects of priori profiles and aerosols on the satellite products, Atmos Chem Phys, 17, 5007-5033, https://doi.org/10.5194/acp-17-5007-2017, 2017.

Wang, Y. P., Wang, Z. F., Yu, C., Zhu, S. Y., Cheng, L. X., Zhang, Y., and Chen, L. F.: Validation of OMI HCHO Products Using MAX-DOAS observations from 2010 to 2016 in Xianghe, Beijing: Investigation of the Effects of Aerosols on
545   Satellite Products, Remote Sens-Basel, 11, 21, https://doi.org/10.3390/rs11020203, 2019.

Xing, C. Z., Liu, C., Hu, Q. H., Fu, Q. Y., Lin, H., Wang, S. T., Su, W. J., Wang, W. W., Javed, Z., and Liu, J. G.: Identifying the wintertime sources of volatile organic compounds (VOCs) from MAX-DOAS measured formaldehyde and glyoxal in Chongqing, southwest China, Sci Total Environ, 715, 12, https://doi.org/10.1016/j.scitotenv.2019.136258, 2020.

550 Xu, J. M., Tie, X. X., Gao, W., Lin, Y. F., and Fu, Q. Y.: Measurement and model analyses of the ozone variation during 2006 to 2015 and its response to emission change in megacity Shanghai, China, Atmos Chem Phys, 19, 9017-9035, https://doi.org/10.5194/acp-19-9017-2019, 2019.

Xue, R. B., Wang, S. S., Li, D. R., Zou, Z., Chan, K. L., Valks, P., Saiz-Lopez, A., and Zhou, B.: Spatio-temporal variations in NO_2 and SO_2 over Shanghai and Chongming Eco-Island measured by Ozone Monitoring Instrument (OMI) during 2008-2017, J Clean Prod, 258, 14, https://doi.org/10.1016/j.jclepro.2020.120563, 2020.

Zaveri, R. A., Berkowitz, C. M., Kleinman, L. I., Springston, S. R., Doskey, P. V., Lonneman, W. A., and Spicer, C. W.: Ozone production efficiency and NO_x depletion in an urban plume: Interpretation of field observations and implications for evaluating O_3-NO_x-VOC sensitivity, J. Geophys. Res.-Atmos., 108, 23, https://doi.org/10.1029/2002jd003144, 2003.

Zhang, C. X., Liu, C., Hu, Q. H., Cai, Z. N., Su, W. J., Xia, C. Z., Zhu, Y. Z., Wang, S. W., and Liu, J. G.: Satellite UV-Vis spectroscopy: implications for air quality trends and their driving forces in China during 2005-2017, Light-Sci Appl, 8, 12, https://doi.org/10.1038/s41377-019-0210-6, 2019.

Zhang, K., Li, L., Huang, L., Wang, Y. J., Huo, J. T., Duan, Y. S., Wang, Y. H., and Fu, Q. Y.: The impact of volatile organic compounds on ozone formation in the suburban area of Shanghai, Atmos Environ, 232, 11, https://doi.org/10.1016/j.atmosenv.2020.117511, 2020.

Zhang, K., Huang, L., Li, Q., Huo, J. T., Duan, Y. S., Wang, Y. H., Yaluk, E., Wang, Y. J., Fu, Q. Y., and Li, L.: Explicit modeling of isoprene chemical processing in polluted air masses in suburban areas of the Yangtze River Delta region: radical cycling and formation of ozone and formaldehyde, Atmos Chem Phys, 21, 5905-5917, https://doi.org/10.5194/acp-21-5905-2021, 2021.

Zhang, Q., Streets, D. G., He, K., Wang, Y., Richter, A., Burrows, J. P., Uno, I., Jang, C. J., Chen, D., Yao, Z., and Lei, Y.: NO_x emission trends for China, 1995-2004: The view from the ground and the view from space, J. Geophys. Res.-Atmos., 112, 18, https://doi.org/10.1029/2007jd008684, 2007.

Zhu, L., Jacob, D. J., Mickley, L. J., Marais, E. A., Cohan, D. S., Yoshida, Y., Duncan, B. N., Abad, G. G., and Chance, K. V.: Anthropogenic emissions of highly reactive volatile organic compounds in eastern Texas inferred from oversampling of satellite (OMI) measurements of HCHO columns, Environ Res Lett, 9, 7, https://doi.org/10.1088/1748-9326/9/11/114004, 2014.

Zhu, L., Jacob, D. J., Keutsch, F. N., Mickley, L. J., Scheffe, R., Strum, M., Abad, G. G., Chance, K., Yang, K., Rappenglück, B., Millet, D. B., Baasandorj, M., Jaegle, L., and Shah, V.: Formaldehyde (HCHO) As a Hazardous Air Pollutant: Mapping Surface Air Concentrations from Satellite and Inferring Cancer Risks in the United States, Environ Sci Technol, 51, 5650-5657, https://doi.org/10.1021/acs.est.7b01356, 2017a.

Zhu, L., Mickley, L. J., Jacob, D. J., Marais, E. A., Sheng, J. X., Hu, L., Abad, G. G., and Chance, K.: Long-term (2005-2014) trends in formaldehyde (HCHO) columns across North America as seen by the OMI satellite instrument: Evidence of changing emissions of volatile organic compounds, Geophys Res Lett, 44, 7079-7086, https://doi.org/10.1002/2017gl073859, 2017b.